A BDF2 energy stable scheme for the binary fluid-surfactant hydrodynamic model

Yuzhe Qin[a,b], Rui Chen[c] and Zhengru Zhang[*b]

[a]*Research Center for Mathematics and Mathematics Education, Beijing Normal University at Zhuhai, 519087, People's Republic of China*
[b]*Laboratory of Mathematics and Complex Systems (Ministry of Education), School of Mathematical Sciences, Beijing Normal University, Beijing 100875, People's Republic of China*
[c]*School of Science, Beijing University of Posts and Telecommunications, Beijing, 100876, People's Republic of China*

Abstract

A second-order time stepping scheme is developed for the binary fluid-surfactant phase field model coupled with hydrodynamics by using the scalar auxiliary variable approach and pressure correction method. The free energy contains a double-well potential, a nonlinear coupling entropy and a Flory-Huggins potential. By introducing one scalar auxiliary variable, the system is transformed into an equivalent form so that the nonlinear terms can be treated semi-explicitly. The scheme is linear and decoupled; thus, they can be solved efficiently. We further prove that the semidiscretized scheme in time is unconditionally energy stable. Numerical experiments are performed to validate the accuracy and energy stability of the proposed scheme.

keywords: binary fluid-surfactant, scalar auxiliary variable approach, pressure correction method, unconditional energy stability, Navier-Stokes equation, BDF2.

1 Introduction

Surfactants move toward the fluid interface in binary fluid due to their amphiphilic structure which contains hydrophile and hydrophobe groups. As a result, they can reduce the interfacial tension and system energy [30]. Surfactants play a very important role in many fields for their property. For example, in biotechnology, surfactants can reduce the risk from bubbles formed in blood due to rapid decompression [2], and in industry applications, surfactants can improve food and shampoo processing and enhance oil recovery [29].

Modeling interfacial dynamics with soluble surfactants in a multiphase system is a challenging task. In the past twenty years, there have been appearing numerous studies related to surfactants [14, 24, 26, 42, 50, 52]. As a matter of fact, there are two fundamental methods of modeling the binary fluid-surfactant system. One of which is the sharp interface model, which has a long history dated back to one century ago [16, 37]. This kind of model is adopted in [21, 23]. In fact, sharp interface models have made great progress in explaining the kinetics of diffusional phase transformations and simulating multiphase systems with surfactants. Nevertheless, there are some difficulties stemming from the interface interactions with various complex processes during the course of phase transformations [29]. The other is the phase field model[13, 25, 15, 43]. Phase field model makes use of an appropriate free energy functional to characterize the interfacial dynamics. This kind of method is adopted to investigate interfacial dynamics with surfactants in [14, 26, 38, 40, 41]. In [26], the phase-field method was used to study the phase transition behaviors of the monolayer microemulsion system, formed by surfactant molecules. Generally, the free energy of the binary fluid-surfactant model consists of the following two parts: The first part is the classical Ginzburg-Landau double well potential, which is used to describe a binary mixture. The other is the nonlinear coupling entropy term to account for the influence of the surfactant in boosting the formation of interfaces. The Ginzburg-Landau double well potential has a historical evolution process for this part of energy. In their pioneering work, Laradji et al. [26] introduced two phase field variables to

---

represent the local densities of the fluids, as well as the local concentration of the surfactant. As mentioned in [24], the authors added an extra diffusion term to prevent the model from becoming unbounded and a Ginzburg-Landau type potential for the concentration variable to allow the coexistence of the two bulk states. To restrict the range of the concentration variable, the authors in [42] added the logarithmic Flory-Huggins potential based on the nonlinear coupling entropy, which is similar to that in [24, 26]. In consideration of penalizing the concentration to accumulate along the fluid interface, the author marginally changed the nonlinear coupled entropy in [14]. In [39], the authors further modified the model in [14] by adding the Flory-Huggins potential for the local concentration variable as well.

In this paper, we focus on constructing a second-order unconditional energy stable numerical scheme for a hydrodynamics coupled binary fluid-surfactant phase-field model [39, 47, 58]. The governing system consists of incompressible Navier-Stokes equations and two Cahn-Hilliard type equations. For the sake of simplicity, many authors work on the partial model, i.e., the phase field model without fluid flow. There have been some excellent studies which focus on numerical approximations for multi-phase models [8, 22]. Owing to the stiff nonlinear terms that originate from the thin interface thickness parameter, there are many difficulties to handle in constructing numerical schemes with unconditional energy stability, especially for the second-order scheme. Many efforts have been made to deal with these problems [8, 48, 55]. The simple fully implicit or explicit type discretization brings extremely severe time step size constraints on the interfacial width [1, 12, 36]. The semi-implicit method is adopted in [39]. However, the author mentioned that the semi-implicit method has a serious constraint on the time step. Lately, Gu et al. [17] constructed an energy stable finite difference scheme for the binary fluid-surfactant system, whose scheme is first order in time based on a convex splitting approach [11, 31, 44, 46]. The scheme managed the convex part of the free energy potential implicitly, while treating the concave part explicitly. There is only first order in time. In addition, algebraic multigrid and Newton-multigrid methods are adopted to solve the linear and nonlinear systems, respectively [17]. More recently, Yang et al. constructed linear and unconditionally energy stable schemes for binary fluid-surfactant systems with constant mobility in [52] using the invariant energy quadratization (IEQ) technique[6, 19, 20, 49, 51, 53, 54, 56]. The free energy is transformed into an equivalent quadratic form by introducing appropriate auxiliary variables. All the nonlinear terms in this system are treated semi-explicitly [52]. Their schemes are linear and unconditionally energy stable. In addition, their schemes can achieve both first-order and second-order accuracy in time. In fact, the IEQ approach leads to a coupled system with a variable coefficient to be solved. Recently, Zhu et al. proposed energy stable schemes in [57] based on the scalar auxiliary variable (SAV) method [34, 35]. Their schemes are decoupled and linear. They introduce two scalar auxiliary variables and demonstrate energy stability for the first-order scheme. Furthermore, they show the energy stability of the second-order scheme by a series of numerical tests. Newly, Shen et al. in [28, 32] proved the convergence and error estimate for the SAV approach for the typical Cahn-Hilliard equation with double-well potential. Here, we focus on the SAV approach to the binary fluid-surfactant system with hydrodynamics, and the numerical analysis will be achieved in our future work.

However, there are numerous excellent works related to phase field models with surfactants. It is extremely difficult to numerically develop unconditionally energy stable schemes for phase-field surfactant models of two-phase incompressible flow. The three difficulties originate from: (1) the strong nonlinear couplings between multiple phase field variables; (2) the coupling between the velocity and multiple phase-field variables through convection terms and nonlinear stresses; and (3) the coupling of the velocity and pressure. When no flow field is considered, the inherent numerical challenges of (2) and (3) are greatly ignored. Compared with the model without flow fields, the hydrodynamic surfactant model is conceivably more complicated for algorithm design. By combining some well-known approaches such as the projection method for Navier-Stokes equations, the scalar auxiliary variable (SAV) approach for nonlinear stiff terms, and implicit-explicit treatments for nonlinear stresses, we obtain a linear, second order, and provably unconditionally energy stable time stepping scheme.

Therefore, in this paper, our primary purpose is to construct a more efficient and effective numerical scheme to solve the binary fluid-surfactant phase field model coupled with hydrodynamics that had been developed in [14, 39, 47]. The proposed scheme is expected to possess the following properties: (1) the theoretical proofs are provided, maintaining the energy dissipation; (2) the proposed second-order scheme in time is efficient and accurate; (3) only several linear systems at each time step need to be solved and are easy to implement. We adopt the SAV approach to deal with nonlinear terms about the phase field variables. The SAV approach is built on the recently introduced IEQ approach. Therefore, the SAV approach inherits all the advantages of the IEQ approach but conquers most of its weaknesses. The IEQ approach will lead to coupled systems with variable coefficients and requires the energy density function to be bounded from below rather than the energy [34]. For the Navier-Stokes equations, we use the pressure correction method to decouple the velocity and pressure. This means that our scheme is

decoupled and easy to implement. Furthermore, we demonstrate unconditional energy stability for the proposed scheme.

The rest of the paper is organized as follows. In Section 2, we give a brief introduction to the hydrodynamical binary fluid surfactant phase field model and its energy law. In Section 3, our numerical scheme with respect to second-order temporal accuracy for this model are presented, and we rigorously prove that the schemes satisfy unconditional energy stability. A certain number of numerical experiments are carried out in Section 4. We present the conclusions of this paper in Section 5.

2 Governing equations and energy law

In this section, we first give a brief description of the hydrodynamic binary fluid-surfactant phase field model developed by [47]. The total free energy for the hydrodynamical binary fluid-surfactant system is given by

$$E\left(\boldsymbol{u}, \phi, \rho\right) = \int_{\Omega} \left(\frac{1}{2}|\boldsymbol{u}|^2 + \frac{f\left(\phi\right)}{\varepsilon} + \frac{\varepsilon}{2}|\nabla\phi|^2 + \frac{\eta}{2}\left|\nabla\rho\right|^2 + \frac{\alpha}{2}\left(\rho - |\nabla\phi|\right)^2 + \beta H\left(\rho\right)\right)\mathrm{d}\boldsymbol{x}, \qquad (2.1)$$

where

$$f\left(\phi\right) = \frac{1}{4}\left(\phi^2 - 1\right)^2, \quad H\left(\rho\right) = \rho\ln\rho + \left(1 - \rho\right)\ln\left(1 - \rho\right).$$

The phase field variables $\phi(\boldsymbol{x}, t)$ and $\rho(\boldsymbol{x}, t)$ are order parameters, where $\phi(\boldsymbol{x}, t) = -1$ or 1 represents two different fluids, and $\rho(\boldsymbol{x}, t)$ describes the local density of the surfactant. There is a thin smooth transition layer between the two different fluids, and the width is described by a small positive constant ε. Thus, the interface of the mixture is represented by the zero level set $\Gamma_t = \{\boldsymbol{x} : \phi(\boldsymbol{x}, t) = 0\}$. In addition, we use $\boldsymbol{u}$ to represent the volume-averaged velocity field. It is clear that we can divide the total free energy functional into four parts and we will give a brief description about them.

$E_k(\boldsymbol{u}) = \int_{\Omega} \frac{1}{2}|\boldsymbol{u}|^2\mathrm{d}\boldsymbol{x}$ is the kinetic energy for the binary mixture fluid-surfactant system. The so-called Cahn-Hilliard energy $E_{CH}\left(\phi\right) = \int_{\Omega}\left(\frac{f(\phi)}{\varepsilon} + \frac{\varepsilon}{2}|\nabla\phi|^2\right)\mathrm{d}\boldsymbol{x}$ is the mixture energy functional describing the coarsening dynamics, where the first term represents the hydrophobic type (tendency of separation) of interactions and the second term in E_{CH} contributes to the hydrophilic type (tendency of mixing) of the interactions between the materials. As a consequence of the competition between the two types of interactions, the equilibrium configuration will include a diffusive interface. Different from [14], an extra energy density $|\nabla\rho|^2$ is added to enhance the stability in entropy $E_{en}\left(\rho\right) = \int_{\Omega}\left(\frac{\eta}{2}\left|\nabla\rho\right|^2 + \beta H\left(\rho\right)\right)\mathrm{d}\boldsymbol{x}$, where η, β are both two small positive constants. $H\left(\rho\right)$ is a Flory-Huggins energy density, and it restricts the value of ρ to be in $(0, 1)$. Finally, the coupled energy functional $E_{cp}\left(\phi, \rho\right) = \int_{\Omega}\frac{\alpha}{2}\left(\rho - |\nabla\phi|\right)^2\mathrm{d}\boldsymbol{x}$, is the penalty term that enables the concentration to accumulate near the interface with a relatively high value.

The equations for the hydrodynamical binary fluid-surfactant phase field model are given as follows:

$$\boldsymbol{u}_t + (\boldsymbol{u}\cdot\nabla)\boldsymbol{u} + \nabla p - \nu\Delta\boldsymbol{u} + \lambda_1\phi\nabla\mu_\phi + \lambda_2\rho\nabla\mu_\rho = 0, \qquad (2.2\text{a})$$

$$\nabla\cdot\boldsymbol{u} = 0, \qquad (2.2\text{b})$$

$$\phi_t + \lambda_1\nabla\cdot(\boldsymbol{u}\phi) = M_1\Delta\mu_\phi, \qquad (2.2\text{c})$$

$$\rho_t + \lambda_2\nabla\cdot(\boldsymbol{u}\rho) = M_2\Delta\mu_\rho, \qquad (2.2\text{d})$$

$$\mu_\phi = \delta_\phi E, \qquad (2.2\text{e})$$

$$\mu_\rho = \delta_\rho E. \qquad (2.2\text{f})$$

We impose the system under the initial conditions as

$$\boldsymbol{u}\left(\boldsymbol{x}, 0\right) = \boldsymbol{u}_0\left(\boldsymbol{x}\right), \phi\left(\boldsymbol{x}, 0\right) = \phi_0\left(\boldsymbol{x}\right), \rho\left(\boldsymbol{x}, 0\right) = \rho_0\left(\boldsymbol{x}\right), \qquad (2.3)$$

and use the following boundary conditions:

$$\boldsymbol{u}\cdot\boldsymbol{n}|_{\partial\Omega} = 0, \ \partial_{\boldsymbol{n}}\phi|_{\partial\Omega} = \partial_{\boldsymbol{n}}\rho|_{\partial\Omega} = 0, \ \partial_{\boldsymbol{n}}\mu_\phi|_{\partial\Omega} = \partial_{\boldsymbol{n}}\mu_\rho|_{\partial\Omega} = 0, \qquad (2.4)$$

where $\boldsymbol{n}$ is the unit outward normal vector of boundary $\partial\Omega$.

The above system $(2.2) - (2.4)$ follows the dissipation law. By taking the L^2 inner products of (2.2a) with $\boldsymbol{u}$, of (2.2c) with μ_ϕ, of ρ with (2.2d) with μ_ρ, of (2.2e) with $-\phi_t$, and of (2.2f) with $-\rho_t$, by using integration by parts and combining all the equalities, we obtain

3

$$\frac{\mathrm{d}}{\mathrm{d}t} E\left(\boldsymbol{u}, \phi, \rho\right) = -\nu\|\nabla\boldsymbol{u}\|^2 - M_1\|\nabla\mu_\phi\|^2 - M_2\|\nabla\mu_\rho\|^2 \le 0. \tag{2.5}$$

Next, our goal is to design a temporal approximation scheme which satisfies the discrete version of the continuous energy law (2.5).

First, we regularize the Flory-Huggins potential from the interval $(0, 1)$ to $\mathbb{R}$. We mainly follow the work in [7]. That is, for any $\xi > 0$, the regularized Flory-Huggins potential is expressed by

$$\hat{H}(\rho) = \begin{cases} \rho\ln\rho + \frac{(1-\rho)^2}{2\xi} + (1-\rho)\ln\xi - \frac{\xi}{2}, & \rho \ge 1 - \xi, \\ \rho\ln\rho + (1-\rho)\ln(1-\rho), & \xi \le \rho \le 1 - \xi, \\ (1-\rho)\ln(1-\rho) + \frac{\rho^2}{2\xi} + \rho\ln\xi - \frac{\xi}{2}, & \rho \le \xi. \end{cases}$$

Notice that when $\xi \to 0$, $\hat{H}(\rho) \to H(\rho)$. We consider the numerical solution to the model formulated with the regularized function $\hat{H}(\rho)$. For convenience, we omit the notation ˆ. Now, we will construct first order and second order numerical schemes in time using the scalar auxiliary variable approach.

Note that

$$E\left(\boldsymbol{u}, \phi, \rho\right) = \int_\Omega \left(\frac{1}{2}|\boldsymbol{u}|^2 + \frac{f(\phi)}{\varepsilon} + \frac{\varepsilon}{2}|\nabla\phi|^2 + \frac{\eta}{2}|\nabla\rho|^2 + \frac{\alpha}{2}\left(\rho - |\nabla\phi|\right)^2 + \beta H(\rho)\right)\mathrm{d}\boldsymbol{x}$$
$$= \int_\Omega \left(\frac{1}{2}|\boldsymbol{u}|^2 + \frac{\varepsilon+\theta}{2}|\nabla\phi|^2 + \frac{\sigma}{2}\phi^2 + \frac{\eta}{2}|\nabla\rho|^2 + \frac{\delta}{2}\rho^2\right)\mathrm{d}\boldsymbol{x} - C$$
$$+ \int_\Omega \left(\frac{f(\phi)}{\varepsilon} + \frac{\alpha}{2}\left(\rho - |\nabla\phi|\right)^2 - \frac{\theta}{2}|\nabla\phi|^2 - \frac{\sigma}{2}\phi^2 - \frac{\delta}{2}\rho^2 + \beta H(\rho)\right)\mathrm{d}\boldsymbol{x} + C,$$

where C is a constant that maintains the nonlinear energy bounded from below. After denoting

$$E_0 = \int_\Omega \left(\frac{f(\phi)}{\varepsilon} + \frac{\alpha}{2}\left(\rho - |\nabla\phi|\right)^2 - \frac{\theta}{2}|\nabla\phi|^2 - \frac{\sigma}{2}\phi^2 - \frac{\delta}{2}\rho^2 + \beta H(\rho)\right)\mathrm{d}\boldsymbol{x} + C \quad \text{and} \quad r(t) = \sqrt{E_0},$$

We have the equivalent equation system as follows:

$$\boldsymbol{u}_t + (\boldsymbol{u}\cdot\nabla)\boldsymbol{u} + \nabla p - \nu\Delta\boldsymbol{u} + \lambda_1\phi\nabla\mu_\phi + \lambda_2\rho\nabla\mu_\rho = 0, \tag{2.6a}$$
$$\nabla\cdot\boldsymbol{u} = 0, \tag{2.6b}$$
$$\phi_t + \lambda_1\nabla\cdot(\boldsymbol{u}\phi) = M_1\Delta\mu_\phi, \tag{2.6c}$$
$$\rho_t + \lambda_2\nabla\cdot(\boldsymbol{u}\rho) = M_2\Delta\mu_\rho, \tag{2.6d}$$
$$\mu_\phi = -(\varepsilon+\theta)\Delta\phi + \sigma\phi + \frac{r}{\sqrt{E_0}}\delta_\phi E_0, \tag{2.6e}$$
$$\mu_\rho = -\eta\Delta\rho + \delta\rho + \frac{r}{\sqrt{E_0}}\delta_\rho E_0, \tag{2.6f}$$
$$r_t = \frac{1}{2\sqrt{E_0}}\left((\delta_\phi E_0, \phi_t) + (\delta_\rho E_0, \rho_t)\right). \tag{2.6g}$$

where

$$\delta_\phi E_0 = \frac{1}{\varepsilon}\left(\phi^2 - 1\right)\phi - (\alpha - \theta)\Delta\phi + \alpha\nabla\cdot\left(\rho\frac{\nabla\phi}{|\nabla\phi|}\right) - \sigma\phi, \tag{2.7}$$
$$\delta_\rho E_0 = (\alpha - \delta)\rho - \alpha|\nabla\phi| + \beta H'(\rho). \tag{2.8}$$

Similar to (2.5), the energy stability is obtained by taking the L^2 inner products of (2.6a) with $\boldsymbol{u}$, of (2.6c) with μ_ϕ, of (2.6d) with (2.6d) with μ_ρ, of (2.6e) with $-\phi_t$, of (2.6f) with $-\rho_t$, and of (2.6g) with $2r$. Using integration by parts and combining all equalities, we obtain

$$\frac{\mathrm{d}}{\mathrm{d}t}\tilde{E}\left(\boldsymbol{u}, \phi, \rho, r\right) = -\nu\|\nabla\boldsymbol{u}\|^2 - M_1\|\nabla\mu_\phi\|^2 - M_2\|\nabla\mu_\rho\|^2 \le 0. \tag{2.9}$$

where

$$\tilde{E}\left(\boldsymbol{u}, \phi, \rho, r\right) = \int_\Omega \left(\frac{1}{2}|\boldsymbol{u}|^2 + \frac{\varepsilon+\theta}{2}|\nabla\phi|^2 + \frac{\sigma}{2}\phi^2 + \frac{\eta}{2}|\nabla\rho|^2 + \frac{\delta}{2}\rho^2\right)\mathrm{d}\boldsymbol{x} - C + r^2$$

is the modified energy functional, which equals the original energy functional.

4

3 Second order unconditionally energy stable numerical scheme

In this section, we use the scalar auxiliary variable approach to decouple the phase field equations and the pressure correction method for the hydrodynamic equations. The resulting system is decoupled and linear.

Step 1: Solve $\left(\phi^{n+1}, \rho^{n+1}, r^{n+1}, \tilde{\boldsymbol{u}}^{n+1}\right)$ using

$$\frac{3\tilde{\boldsymbol{u}}^{n+1} - 4\boldsymbol{u}^n + \boldsymbol{u}^{n-1}}{2\Delta t} + B\left(\hat{\boldsymbol{u}}^{n+1}, \tilde{\boldsymbol{u}}^{n+1}\right) + \nabla p^n - \nu\Delta\tilde{\boldsymbol{u}}^{n+1} + \lambda_1\hat{\phi}^{n+1}\nabla\mu_\phi^{n+1} + \lambda_2\hat{\rho}^{n+1}\nabla\mu_\rho^{n+1} = 0, \tag{3.1a}$$

$$\frac{3\phi^{n+1} - 4\phi^n + \phi^{n-1}}{2\Delta t} + \lambda_1\nabla\cdot\left(\tilde{\boldsymbol{u}}^{n+1}\hat{\phi}^{n+1}\right) = M_1\Delta\mu_\phi^{n+1}, \tag{3.1b}$$

$$\frac{3\rho^{n+1} - 4\rho^n + \rho^{n-1}}{2\Delta t} + \lambda_2\nabla\cdot\left(\tilde{\boldsymbol{u}}^{n+1}\hat{\rho}^{n+1}\right) = M_2\Delta\mu_\rho^{n+1}, \tag{3.1c}$$

$$\mu_\phi^{n+1} = -\left(\varepsilon + \theta\right)\Delta\phi^{n+1} + \sigma\phi^{n+1} + V_\phi^n r^{n+1}, \tag{3.1d}$$

$$\mu_\rho^{n+1} = -\eta\Delta\rho^{n+1} + \delta\rho^{n+1} + V_\rho^n r^{n+1}, \tag{3.1e}$$

$$3r^{n+1} - 4r^n + r^{n-1} = \frac{1}{2}\left(V_\phi^n, 3\phi^{n+1} - 4\phi^n + \phi^{n-1}\right) + \frac{1}{2}\left(V_\rho^n, 3\rho^{n+1} - 4\rho^n + \rho^{n-1}\right), \tag{3.1f}$$

where

$$B\left(\boldsymbol{u}, \boldsymbol{v}\right) = \left(\boldsymbol{u}\cdot\nabla\right)\boldsymbol{v} + \frac{1}{2}\left(\nabla\cdot\boldsymbol{u}\right)\boldsymbol{v},$$

$$\hat{\boldsymbol{u}}^{n+1} = 2\boldsymbol{u}^n - \boldsymbol{u}^{n-1}, \quad \hat{\phi}^{n+1} = 2\phi^n - \phi^{n-1}, \quad \hat{\rho}^{n+1} = 2\rho^n - \rho^{n-1},$$

$$V_\phi^n = \frac{\delta_\phi E_0\left(\hat{\phi}^{n+1}, \hat{\rho}^{n+1}\right)}{\sqrt{E_0\left(\hat{\phi}^{n+1}, \hat{\rho}^{n+1}\right)}}, \quad V_\rho^n = \frac{\delta_\rho E_0\left(\hat{\phi}^{n+1}, \hat{\rho}^{n+1}\right)}{\sqrt{E_0\left(\hat{\phi}^{n+1}, \hat{\rho}^{n+1}\right)}},$$

and the boundary condition is as follows:

$$\tilde{\boldsymbol{u}}^{n+1}|_{\partial\Omega} = 0, \; \partial_{\boldsymbol{n}}\phi^{n+1}|_{\partial\Omega} = \partial_{\boldsymbol{n}}\rho^{n+1}|_{\partial\Omega} = 0, \; \partial_{\boldsymbol{n}}\mu_\phi^{n+1}|_{\partial\Omega} = \partial_{\boldsymbol{n}}\mu_\rho^{n+1}|_{\partial\Omega} = 0. \tag{3.2}$$

From equation (3.1f), we have

$$r^{n+1} = \frac{4}{3}r^n - \frac{1}{3}r^{n-1} + \frac{1}{2}\left(V_\phi^n, \phi^{n+1} - \frac{4}{3}\phi^n + \frac{1}{3}\phi^{n-1}\right) + \frac{1}{2}\left(V_\rho^n, \rho^{n+1} - \frac{4}{3}\rho^n + \frac{1}{3}\rho^{n-1}\right). \tag{3.3}$$

We substitute (3.3) into (3.1d) and (3.1e), respectively, then we obtain

$$\mu_\phi^{n+1} = -(\varepsilon + \theta)\Delta\phi^{n+1} + \sigma\phi^{n+1} + V_\phi^n\Big[\frac{4}{3}r^n - \frac{1}{3}r^{n-1}$$
$$+ \frac{1}{2}\left(V_\phi^n, \phi^{n+1} - \frac{4}{3}\phi^n + \frac{1}{3}\phi^{n-1}\right) + \frac{1}{2}\left(V_\rho^n, \rho^{n+1} - \frac{4}{3}\rho^n + \frac{1}{3}\rho^{n-1}\right)\Big], \tag{3.4a}$$

$$\mu_\rho^{n+1} = -\eta\Delta\rho^{n+1} + \delta\rho^{n+1} + V_\rho^n\Big[\frac{4}{3}r^n - \frac{1}{3}r^{n-1}$$
$$+ \frac{1}{2}\left(V_\phi^n, \phi^{n+1} - \frac{4}{3}\phi^n + \frac{1}{3}\phi^{n-1}\right) + \frac{1}{2}\left(V_\rho^n, \rho^{n+1} - \frac{4}{3}\rho^n + \frac{1}{3}\rho^{n-1}\right)\Big]. \tag{3.4b}$$

When we substitute (3.4a) and (3.4b) into (3.1b) and (3.1c) respectively, it gives

$$\frac{3\phi^{n+1} - 4\phi^n + \phi^{n-1}}{2\Delta t} + \lambda_1\nabla\cdot\left(\tilde{\boldsymbol{u}}^{n+1}\hat{\phi}^{n+1}\right) = -(\varepsilon + \theta)M_1\Delta^2\phi^{n+1} + M_1\sigma\Delta\phi^{n+1}$$
$$+ M_1\Delta V_\phi^n\Big[\frac{4}{3}r^n - \frac{1}{3}r^{n-1} + \frac{1}{2}\left(V_\phi^n, \phi^{n+1} - \frac{4}{3}\phi^n + \frac{1}{3}\phi^{n-1}\right) + \frac{1}{2}\left(V_\rho^n, \rho^{n+1} - \frac{4}{3}\rho^n + \frac{1}{3}\rho^{n-1}\right)\Big],$$

$$\frac{3\rho^{n+1} - 4\rho^n + \rho^{n-1}}{2\Delta t} + \lambda_2\nabla\cdot\left(\tilde{\boldsymbol{u}}^{n+1}\hat{\rho}^{n+1}\right) = -\eta M_2\Delta^2\rho^{n+1} + M_2\delta\Delta\rho^{n+1}$$
$$+ M_2\Delta V_\rho^n\Big[\frac{4}{3}r^n - \frac{1}{3}r^{n-1} + \frac{1}{2}\left(V_\phi^n, \phi^{n+1} - \frac{4}{3}\phi^n + \frac{1}{3}\phi^{n-1}\right) + \frac{1}{2}\left(V_\rho^n, \rho^{n+1} - \frac{4}{3}\rho^n + \frac{1}{3}\rho^{n-1}\right)\Big],$$

and we have

$$\left[I + \frac{2\Delta t\,(\varepsilon+\theta)\,M_1}{3}\Delta^2 - \frac{2\Delta t M_1\sigma}{3}\Delta\right]\phi^{n+1} - \frac{\Delta t M_1}{3}\left[(V_\phi^n,\phi^{n+1}) + (V_\rho^n,\rho^{n+1})\right]\Delta V_\phi^n + \frac{2\Delta t}{3}\lambda_1\nabla\cdot(\tilde{\boldsymbol{u}}^{n+1}\hat{\phi}^{n+1})$$
$$=\frac{4}{3}\phi^n - \frac{1}{3}\phi^{n-1} + \frac{2\Delta t M_1}{3}\left[\frac{4}{3}r^n - \frac{1}{3}r^{n-1} + \frac{1}{2}\left(V_\phi^n, -\frac{4}{3}\phi^n + \frac{1}{3}\phi^{n-1}\right) + \frac{1}{2}\left(V_\rho^n, -\frac{4}{3}\rho^n + \frac{1}{3}\rho^{n-1}\right)\right]\Delta V_\phi^n = g_\phi^n,$$

$$\left[I + \frac{2\Delta t\eta M_2}{3}\Delta^2 - \frac{2\Delta t M_2}{3}\delta\Delta\right]\phi^{n+1} - \frac{\Delta t M_2}{3}\left[(V_\phi^n,\phi^{n+1}) + (V_\rho^n,\rho^{n+1})\right]\Delta V_\rho^n + \frac{2\Delta t}{3}\lambda_2\nabla\cdot(\tilde{\boldsymbol{u}}^{n+1}\hat{\rho}^{n+1})$$
$$=\frac{4}{3}\rho^n - \frac{1}{3}\rho^{n-1} + \frac{2\Delta t M_2}{3}\left[\frac{4}{3}r^n - \frac{1}{3}r^{n-1} + \frac{1}{2}\left(V_\phi^n, -\frac{4}{3}\phi^n + \frac{1}{3}\phi^{n-1}\right) + \frac{1}{2}\left(V_\rho^n, -\frac{4}{3}\rho^n + \frac{1}{3}\rho^{n-1}\right)\right]\Delta V_\rho^n = g_\rho^n.$$

Denoting

$$\mathcal{A} = I + \frac{2\Delta t\,(\varepsilon+\theta)\,M_1}{3}\Delta^2 - \frac{2\Delta t M_1}{3}\sigma\Delta, \quad \mathcal{B} = I + \frac{2\Delta t\eta M_2}{3}\Delta^2 - \frac{2\Delta t M_2}{3}\delta\Delta,$$

we have

$$\mathcal{A}\phi^{n+1} - \frac{\Delta t M_1}{3}\left[(V_\phi^n,\phi^{n+1}) + (V_\rho^n,\rho^{n+1})\right]\Delta V_\phi^n + \frac{2\Delta t}{3}\lambda_1\nabla\cdot(\tilde{\boldsymbol{u}}^{n+1}\hat{\phi}^{n+1}) = g_\phi^n,$$
$$\mathcal{B}\rho^{n+1} - \frac{\Delta t M_2}{3}\left[(V_\phi^n,\phi^{n+1}) + (V_\rho^n,\rho^{n+1})\right]\Delta V_\rho^n + \frac{2\Delta t}{3}\lambda_2\nabla\cdot(\tilde{\boldsymbol{u}}^{n+1}\hat{\rho}^{n+1}) = g_\rho^n,$$

and thus

$$\phi^{n+1} - \frac{\Delta t M_1}{3}\left[(V_\phi^n,\phi^{n+1}) + (V_\rho^n,\rho^{n+1})\right]\mathcal{A}^{-1}\Delta V_\phi^n + \frac{2\Delta t}{3}\lambda_1\mathcal{A}^{-1}\nabla\cdot(\tilde{\boldsymbol{u}}^{n+1}\hat{\phi}^{n+1}) = \mathcal{A}^{-1}g_\phi^n, \quad (3.6a)$$
$$\rho^{n+1} - \frac{\Delta t M_2}{3}\left[(V_\phi^n,\phi^{n+1}) + (V_\rho^n,\rho^{n+1})\right]\mathcal{B}^{-1}\Delta V_\rho^n + \frac{2\Delta t}{3}\lambda_2\mathcal{B}^{-1}\nabla\cdot(\tilde{\boldsymbol{u}}^{n+1}\hat{\rho}^{n+1}) = \mathcal{B}^{-1}g_\rho^n. \quad (3.6b)$$

After taking the L^2 inner product of (3.6a) with V_ϕ^n and of (3.6b) with V_ρ^n, we have

$$(V_\phi^n,\phi^{n+1}) - \frac{\Delta t M_1}{3}[(V_\phi^n,\phi^{n+1}) + (V_\rho^n,\rho^{n+1})](V_\phi^n,\mathcal{A}^{-1}\Delta V_\phi^n) + \frac{2\Delta t}{3}\lambda_1(V_\phi^n,\mathcal{A}^{-1}\nabla\cdot(\tilde{\boldsymbol{u}}^{n+1}\hat{\phi}^{n+1})) = (V_\phi^n,\mathcal{A}^{-1}g_\phi^n),$$
$$(V_\rho^n,\rho^{n+1}) - \frac{\Delta t M_2}{3}[(V_\phi^n,\phi^{n+1}) + (V_\rho^n,\rho^{n+1})](V_\rho^n,\mathcal{B}^{-1}\Delta V_\rho^n) + \frac{2\Delta t}{3}\lambda_2(V_\rho^n,\mathcal{B}^{-1}\nabla\cdot(\tilde{\boldsymbol{u}}^{n+1}\hat{\rho}^{n+1})) = (V_\rho^n,\mathcal{B}^{-1}g_\rho^n),$$

then we obtain

$$\left[I - \frac{\Delta t M_1}{3}\left(V_\phi^n,\mathcal{A}^{-1}\Delta V_\phi^n\right) - \frac{\Delta t M_2}{3}\left(V_\rho^n,\mathcal{B}^{-1}\Delta V_\rho^n\right)\right]\left[(V_\phi^n,\phi^{n+1}) + (V_\rho^n,\rho^{n+1})\right]$$
$$+ \frac{2\Delta t}{3}\lambda_1\left(V_\phi^n,\mathcal{A}^{-1}\nabla\cdot(\tilde{\boldsymbol{u}}^{n+1}\hat{\phi}^{n+1})\right) + \frac{2\Delta t}{3}\lambda_2\left(V_\rho^n,\mathcal{B}^{-1}\nabla\cdot(\tilde{\boldsymbol{u}}^{n+1}\hat{\rho}^{n+1})\right) = \left(V_\phi^n,\mathcal{A}^{-1}g_\phi^n\right) + \left(V_\rho^n,\mathcal{B}^{-1}g_\rho^n\right).$$

Up to now, the following equations need to be solved

$$\mathcal{A}^{-1}\Delta V_\phi^n, \quad \mathcal{A}^{-1}\nabla\cdot(\tilde{\boldsymbol{u}}^{n+1}\hat{\phi}^{n+1}), \quad \mathcal{A}^{-1}g_\phi^n,$$
$$\mathcal{B}^{-1}\Delta V_\rho^n, \quad \mathcal{B}^{-1}\nabla\cdot(\tilde{\boldsymbol{u}}^{n+1}\hat{\rho}^{n+1}), \quad \mathcal{B}^{-1}g_\rho^n,$$

which requires solving 6 linear equations. Then, we can obtain $\tilde{\boldsymbol{u}}^{n+1}$ by the following equation:

$$\tilde{\boldsymbol{u}}^{n+1} + \frac{2\Delta t}{3}B\left(\hat{\boldsymbol{u}}^{n+1},\tilde{\boldsymbol{u}}^{n+1}\right) - \frac{2\Delta t}{3}\nu\Delta\tilde{\boldsymbol{u}}^{n+1} = \frac{4}{3}\boldsymbol{u}^n - \frac{1}{3}\boldsymbol{u}^{n-1} - \frac{2\Delta t}{3}\left(\nabla p^n + \hat{\phi}^{n+1}\nabla\mu_\phi^{n+1} + \hat{\rho}^{n+1}\nabla\mu_\rho^{n+1}\right).$$

Step 2: We solve $(\tilde{\boldsymbol{u}}^{n+1}, p^{n+1})$ using

$$3\frac{\boldsymbol{u}^{n+1} - \tilde{\boldsymbol{u}}^{n+1}}{2\Delta t} + \nabla\left(p^{n+1} - p^n\right) = 0, \tag{3.7a}$$
$$\nabla\cdot\boldsymbol{u}^{n+1} = 0, \tag{3.7b}$$

with the boundary condition $\boldsymbol{u}^{n+1}\cdot\boldsymbol{n}|_{\partial\Omega} = 0$. We only need to solve the following linear equation.

$$\frac{3}{2\Delta t}\nabla\cdot\left(\boldsymbol{u}^{n+1} - \tilde{\boldsymbol{u}}^{n+1}\right) + \Delta\left(p^{n+1} - p^n\right) = 0.$$

We frequently use the following equation in the proof of the energy stability of the scheme.

$$2\left(a^{n+1}, 3a^{n+1} - 4a^n + a^{n-1}\right) = |a^{n+1}|^2 + |2a^{n+1} - a^n|^2 - |a^n|^2 - |2a^n - a^{n-1}|^2 + |a^{n+1} - 2a^n + a^{n-1}|^2.$$

Theorem 3.1. *The second-order linear scheme* (3.1a) − (3.7b) *is unconditionally energy stable, i.e.; it satisfies the following discrete energy dissipation law:*

$$\frac{1}{\Delta t}\left(E_{2nd}^{n+1,n} - E_{2nd}^{n,n-1}\right) \leq -M_1\Delta t\|\nabla\mu_\phi^{n+1}\|^2 - M_2\Delta t\|\nabla\mu_\rho^{n+1}\|^2 - \gamma\Delta t\|\nabla\tilde{\boldsymbol{u}}^{n+1}\|^2 \leq 0, \qquad (3.8)$$

where

$$
\begin{aligned}
E_{2nd}^{n+1,n} =& \frac{\varepsilon+\theta}{4}\left(\|\nabla\phi^{n+1}\|^2 + \|2\nabla\phi^{n+1} - \nabla\phi^n\|^2\right) + \frac{\sigma}{4}\left(\|\phi^{n+1}\|^2 + \|2\phi^{n+1} - \phi^n\|^2\right) \\
&+ \frac{\eta}{4}\left(\|\nabla\rho^{n+1}\|^2 + \|2\nabla\rho^{n+1} - \nabla\rho^n\|^2\right) + \frac{\delta}{4}\left(\|\rho^{n+1}\|^2 + \|2\rho^{n+1} - \rho^n\|^2\right) \\
&+ \frac{1}{2}\left(|r^{n+1}|^2 + |2r^{n+1} - r^n|^2\right) + \frac{1}{4}\left(\|\boldsymbol{u}^{n+1}\|^2 + \|2\boldsymbol{u}^{n+1} - \boldsymbol{u}^n\|^2\right) + \frac{\Delta t^2}{3}\|\nabla p^{n+1}\|^2.
\end{aligned}
$$

Proof. First, we take the L^2 inner product of equations (3.1b), (3.1c), (3.1d), (3.1e) with $2\Delta t\mu_\phi^{n+1}$, $2\Delta t\mu_\rho^{n+1}$, $3\phi^{n+1} - 4\phi^n + \phi^{n-1}$, $3\rho^{n+1} - 4\rho^n + \rho^{n-1}$ respectively. Multiplying (3.1f) by $2r^{n+1}$ yields

$$(3\phi^{n+1} - 4\phi^n + \phi^{n-1}, \mu_\phi^{n+1}) + 2\Delta t\lambda_1(\tilde{\boldsymbol{u}}^{n+1}, \hat{\phi}^{n+1}\nabla\mu_\phi^{n+1}) - 2M_1\Delta t\|\nabla\mu_\phi^{n+1}\|^2, \qquad (3.9)$$

$$(3\rho^{n+1} - 4\rho^n + \rho^{n-1}, \mu_\rho^{n+1}) + 2\Delta t\lambda_2(\tilde{\boldsymbol{u}}^{n+1}, \hat{\rho}^{n+1}\nabla\mu_\rho^{n+1}) = -2M_2\Delta t\|\nabla\mu_\rho^{n+1}\|^2, \qquad (3.10)$$

$$
\begin{aligned}
&\left(3\phi^{n+1} - 4\phi^n + \phi^{n-1}, \mu_\phi^{n+1}\right) \\
=& \left(3\phi^{n+1} - 4\phi^n + \phi^{n-1}, -(\varepsilon+\theta)\Delta\phi^{n+1} + \sigma\phi^{n+1}\right) + \left(3\phi^{n+1} - 4\phi^n + \phi^{n-1}, V_\phi^n r^{n+1}\right) \\
=& \frac{\varepsilon+\theta}{2}\big(\|\nabla\phi^{n+1}\|^2 + \|2\nabla\phi^{n+1} - \nabla\phi^n\|^2 - \|\nabla\phi^n\|^2 - \|2\nabla\phi^n - \nabla\phi^{n-1}\|^2 + \|\nabla\phi^{n+1} - 2\nabla\phi^n + \nabla\phi^{n-1}\|^2\big) \\
&+ \frac{\sigma}{2}\big(\|\phi^{n+1}\|^2 + \|2\phi^{n+1} - \phi^n\|^2 - \|\phi^n\|^2 - \|2\phi^n - \phi^{n-1}\|^2 + \|\phi^{n+1} - \phi^n + \phi^{n-1}\|^2\big) \\
&+ \left(3\phi^{n+1} - 4\phi^n + \phi^{n-1}, V_\phi^n r^{n+1}\right),
\end{aligned}
\qquad (3.11)
$$

$$
\begin{aligned}
&\left(3\rho^{n+1} - 4\rho^n + \rho^{n-1}, \mu_\rho^{n+1}\right) \\
=& \left(3\rho^{n+1} - 4\rho^n + \rho^{n-1}, -\eta\Delta\rho^{n+1} + \delta\rho^{n+1}\right) + \left(3\rho^{n+1} - 4\rho^n + \rho^{n-1}, V_\rho^n r^{n+1}\right) \\
=& \frac{\eta}{2}\big(\|\nabla\rho^{n+1}\|^2 + \|2\nabla\rho^{n+1} - \nabla\rho^n\|^2 - \|\nabla\rho^n\|^2 - \|2\nabla\rho^n - \nabla\rho^{n-1}\|^2 + \|\nabla\rho^{n+1} - 2\nabla\rho^n + \nabla\rho^{n-1}\|^2\big) \\
&+ \frac{\delta}{2}\Big(\|\rho^{n+1}\|^2 + \|2\rho^{n+1} - \rho^n\|^2 - \|\rho^n\|^2 - \|2\rho^n - \rho^n\|^2 + \|\rho^{n+1} - 2\rho^n + \rho^{n-1}\|^2\Big) \\
&+ \left(3\rho^{n+1} - 4\rho^n + \rho^{n-1}, V_\rho^n r^{n+1}\right),
\end{aligned}
\qquad (3.12)
$$

$$
\begin{aligned}
&\left(V_\phi^n r^{n+1}, 3\phi^{n+1} - 4\phi^n + \phi^{n-1}\right) + \left(V_\phi^n r^{n+1}, 3\phi^{n+1} - 4\phi^n + \phi^{n-1}\right) \\
=& 2r^{n+1}\left(3r^{n+1} - 4r^n + r^{n-1}\right) \\
=& |r^{n+1}|^2 + |2r^{n+1} - r^n|^2 - |r^n|^2 - |2r^n - r^{n-1}|^2 + |r^{n+1} - 2r^n + r^{n-1}|^2.
\end{aligned}
\qquad (3.13)
$$

Then, we take the L^2 inner product of (2.6a) with $2\Delta t\tilde{\boldsymbol{u}}^{n+1}$, and we obtain

$$
\begin{aligned}
\left(3\tilde{\boldsymbol{u}}^{n+1} - 4\boldsymbol{u}^n + \boldsymbol{u}^{n-1}, \tilde{\boldsymbol{u}}^{n+1}\right) + 2\gamma\Delta t\|\nabla\tilde{\boldsymbol{u}}^{n+1}\|^2 + 2\Delta t\left(\nabla p^n, \tilde{\boldsymbol{u}}^{n+1}\right) \\
+ 2\Delta t\lambda_1\left(\hat{\phi}^{n+1}\nabla\mu_\phi^{n+1}, \tilde{\boldsymbol{u}}^{n+1}\right) + 2\Delta t\lambda_2\left(\hat{\rho}^{n+1}\nabla\mu_\rho^{n+1}, \tilde{\boldsymbol{u}}^{n+1}\right) = 0.
\end{aligned}
\qquad (3.14)
$$

From (3.7a), for any function $\boldsymbol{v}$ with $\nabla \cdot \boldsymbol{v} = 0$, we can derive

$$(\boldsymbol{u}^{n+1}, \boldsymbol{v}) = (\tilde{\boldsymbol{u}}^{n+1}, \boldsymbol{v}).$$

Then, for the first term in (3.14), we have

$$
\begin{aligned}
&\left(3\tilde{\boldsymbol{u}}^{n+1} - 4\boldsymbol{u}^n + \boldsymbol{u}^{n-1}, \tilde{\boldsymbol{u}}^{n+1}\right) \\
=& \left(3\tilde{\boldsymbol{u}}^{n+1} - 4\boldsymbol{u}^n + \boldsymbol{u}^{n-1}, \boldsymbol{u}^{n+1}\right) + \left(3\tilde{\boldsymbol{u}}^{n+1} - 4\boldsymbol{u}^n + \boldsymbol{u}^{n-1}, \tilde{\boldsymbol{u}}^{n+1} - \boldsymbol{u}^{n+1}\right) \\
=& \left(3\tilde{\boldsymbol{u}}^{n+1} - 4\boldsymbol{u}^n + \boldsymbol{u}^{n-1}, \boldsymbol{u}^{n+1}\right) + \left(3\tilde{\boldsymbol{u}}^{n+1}, \tilde{\boldsymbol{u}}^{n+1} - \boldsymbol{u}^{n+1}\right) \\
=& \left(3\boldsymbol{u}^{n+1} - 4\boldsymbol{u}^n + \boldsymbol{u}^{n-1}, \boldsymbol{u}^{n+1}\right) + 3\left(\tilde{\boldsymbol{u}}^{n+1} + \boldsymbol{u}^{n+1}, \tilde{\boldsymbol{u}}^{n+1} - \boldsymbol{u}^{n+1}\right) \\
=& \frac{1}{2}\left(\|\boldsymbol{u}^{n+1}\|^2 - \|\boldsymbol{u}^n\|^2 + \|2\boldsymbol{u}^{n+1} - \boldsymbol{u}^n\|^2 - \|2\boldsymbol{u}^n - \boldsymbol{u}^{n-1}\|^2 + \|\boldsymbol{u}^{n+1} - 2\boldsymbol{u}^n + \boldsymbol{u}^{n-1}\|^2\right) \\
&+ 3\left(\|\tilde{\boldsymbol{u}}^{n+1}\|^2 - \|\boldsymbol{u}^{n+1}\|^2\right).
\end{aligned}
$$

For the projection step, we rewrite (3.7a) as

$$\frac{3}{2\Delta t}\boldsymbol{u}^{n+1} + \nabla p^{n+1} = \frac{3}{2\Delta t}\tilde{\boldsymbol{u}}^{n+1} + \nabla p^n.$$

By squaring both sides of the above equality, we obtain

$$\frac{9}{4\Delta t^2}\|\boldsymbol{u}^{n+1}\|^2 + \|\nabla p^{n+1}\|^2 = \frac{9}{4\Delta t^2}\|\tilde{\boldsymbol{u}}^{n+1}\|^2 + \|\nabla p^{n+1}\|^2 + \frac{3}{\Delta t}\left(\tilde{\boldsymbol{u}}^{n+1}, \nabla p\right).$$

namely, by multiplying by $2\Delta t^2/3$, we have

$$\frac{3}{2}\left(\|\boldsymbol{u}^{n+1}\|^2 - \|\tilde{\boldsymbol{u}}^{n+1}\|^2\right) + \frac{2\Delta t^2}{3}\left(\|\nabla p^{n+1}\|^2 - \|\nabla p^n\|^2\right) = 2\Delta t\left(\tilde{\boldsymbol{u}}^{n+1}, \nabla p\right).$$

By taking the L^2 inner product of (3.7a) with $2\Delta t\boldsymbol{u}^{n+1}$, we have

$$\frac{3}{2}\left(\|\boldsymbol{u}^{n+1}\|^2 - \|\tilde{\boldsymbol{u}}^{n+1}\|^2 + \|2\boldsymbol{u}^{n+1} - \tilde{\boldsymbol{u}}^{n+1}\|^2\right) = 0.$$

Combinating the above equations gives

$$\frac{1}{2}\left(\|\boldsymbol{u}^{n+1}\|^2 - \|\boldsymbol{u}^n\|^2 + \|2\boldsymbol{u}^{n+1} - \boldsymbol{u}^n\|^2 - \|2\boldsymbol{u}^n - \boldsymbol{u}^{n-1}\|^2 + \|\boldsymbol{u}^{n+1} - 2\boldsymbol{u}^n + \boldsymbol{u}^{n-1}\|^2\right)$$

$$+ 2\gamma\Delta t\|\nabla\tilde{\boldsymbol{u}}^{n+1}\|^2 + \frac{3}{2}\|\boldsymbol{u}^{n+1} - \tilde{\boldsymbol{u}}^{n+1}\|^2 + \frac{2\Delta t^2}{3}\left(\|\nabla p^{n+1}\|^2 - \|\nabla p^n\|^2\right)$$

$$+ 2\Delta t\lambda_1(\hat{\phi}^{n+1}\nabla\mu_\phi^{n+1}, \tilde{\boldsymbol{u}}^{n+1}) + 2\Delta t\lambda_2(\hat{\rho}^{n+1}\nabla\mu_\rho^{n+1}, \tilde{\boldsymbol{u}}^{n+1}) = 0. \tag{3.15}$$

The combination of $(3.9), (3.10), (3.11), (3.12), (3.13)$ and (3.15) gives us

$$\frac{\varepsilon + \theta}{2}\left(\|\nabla\phi^{n+1}\|^2 + \|2\nabla\phi^{n+1} - \nabla\phi^n\|^2 - \|\nabla\phi^n\|^2 - \|2\nabla\phi^n - \nabla\phi^{n-1}\|^2 + \|\nabla\phi^{n+1} - 2\nabla\phi^n + \nabla\phi^{n-1}\|^2\right)$$

$$+ \frac{\sigma}{2}\left(\|\phi^{n+1}\|^2 + \|2\phi^{n+1} - \phi^n\|^2 - \|\phi^n\|^2 - \|2\phi^n - \phi^{n-1}\|^2 + \|\phi^{n+1} - \phi^n + \phi^{n-1}\|^2\right)$$

$$+ \frac{\eta}{2}\left(\|\nabla\rho^{n+1}\|^2 + \|2\nabla\rho^{n+1} - \nabla\rho^n\|^2 - \|\nabla\rho^n\|^2 - \|2\nabla\rho^n - \nabla\rho^{n-1}\|^2 + \|\nabla\rho^{n+1} - 2\nabla\rho^n + \nabla\rho^{n-1}\|^2\right)$$

$$+ \frac{\delta}{2}\left(\|\rho^{n+1}\|^2 + \|2\rho^{n+1} - \rho^n\|^2 - \|\rho^n\|^2 - \|2\rho^n - \rho^n\|^2 + \|\rho^{n+1} - 2\rho^n + \rho^{n-1}\|^2\right)$$

$$+ \left(|r^{n+1}|^2 + |2r^{n+1} - r^n|^2 - |r^n|^2 - |2r^n - r^{n-1}|^2 + |r^{n+1} - 2r^n + r^{n-1}|^2\right)$$

$$+ \frac{1}{2}\left(\|\boldsymbol{u}^{n+1}\|^2 - \|\boldsymbol{u}^n\|^2 + \|2\boldsymbol{u}^{n+1} - \boldsymbol{u}^n\|^2 - \|2\boldsymbol{u}^n - \boldsymbol{u}^{n-1}\|^2 + \|\boldsymbol{u}^{n+1} - 2\boldsymbol{u}^n + \boldsymbol{u}^{n-1}\|^2\right)$$

$$+ \frac{3}{2}\|\boldsymbol{u}^{n+1} - \tilde{\boldsymbol{u}}^{n+1}\|^2 + \frac{2\Delta t^2}{3}\left(\|\nabla p^{n+1}\|^2 - \|\nabla p^n\|^2\right)$$

$$= -2M_1\Delta t\|\nabla\mu_\phi^{n+1}\|^2 - 2M_2\Delta t\|\nabla\mu_\rho^{n+1}\|^2 - 2\gamma\Delta t\|\nabla\tilde{\boldsymbol{u}}^{n+1}\|^2 \le 0.$$

Finally, we obtain the result (3.8) after dropping some positive terms from the above equation. $\qquad\square$

Remark 3.1. *In theorem 3.1, we only prove the energy stability about the modified energy functional. There is no strict proof for the energy stability about the original energy functional with the SAV approach. However, first, in the numerical result, we will find that the original and modified energy functional have the same decay tendency, and we will give the corresponding numerical results in Figure 1 and 2. In fact, the modified energy functional is the same as the original energy functional in the sense of continuity. We believe the modified energy functional is an approximation of the original energy functional in the discrete sense. Second, in recent work [5], the authors propose a new Lagrange multiplier approach for gradient flows, and a theoretical result for the stability of the original energy is given. We will study the theoretical result for this approximation. In addition, convex splitting is a constructive method for establishing an energy stable numerical scheme. We will also consider using this method to construct an energy stable scheme for the original energy functional.*

Remark 3.2. *Since the function ρ represents the density of surfactant, it is necessary that we must keep the value of ρ bounded in $(0, 1)$. Giving theoretical justification for the positivity-preserving property is valuable. However, this is a challenging analysis, and we will consider this property in our future work. Additionally, there have been a few existing works to establish the positivity-preserving property for the gradient flow with the logarithmic Flory-Huggins energy potential using the convex splitting approaches, such as [4, 9, 10]. There are some excellent resources related to bound preserving [18, 33]. We will refer to these associated analyses in our future work.*

Remark 3.3. *Undoubtedly, unconditional energy stability is an important property in the computation of gradient flows. However, we cannot neglect other properties, such as the convergence and stability. There is some excellent work related to numerical analysis for gradient flows with the SAV approach, such as [3, 27, 32]. However, we cannot obtain these hydrodynamic properties for binary fluid-surfactant phase field model with the SAV approach. To date, there is no more work about the theoretical numerical analysis of this model. because of its strong singularity and coupling. We will consider the error estimates of the binary fluid-surfactant phase field model in our future work.*

Remark 3.4. *One can also easily develop an alternative version of the second-order scheme based on the Crank-Nicolson-type scheme. Assuming that ϕ^{n-1}, ρ^{n-1}, $\boldsymbol{u}^{n-1}$ and ϕ^n, ρ^n, and $\boldsymbol{u}^n$ are known, then we can derive ϕ^{n+1}, ρ^{n+1}, and $\boldsymbol{u}^{n+1}$ with the following system.*

Step 1: *We can obtain ϕ^{n+1}, ρ^{n+1}, and $\tilde{\boldsymbol{u}}^{n+1}$ by using the following equations:*

$$\frac{\tilde{\boldsymbol{u}}^{n+1} - \boldsymbol{u}^n}{\Delta t} + B(\check{\boldsymbol{u}}, \tilde{\boldsymbol{u}}^{n+\frac{1}{2}}) + \nabla p^n - \nu \Delta \tilde{\boldsymbol{u}}^{n+\frac{1}{2}} + \lambda_1 \check{\phi} \nabla \mu_\phi^{n+\frac{1}{2}} + \lambda_2 \check{\rho} \nabla \mu_\rho^{n+\frac{1}{2}} = 0, \tag{3.16a}$$

$$\frac{\phi^{n+1} - \phi^n}{\Delta t} + \lambda_1 \nabla \cdot (\tilde{\boldsymbol{u}}^{n+\frac{1}{2}} \check{\phi}) = M_1 \Delta \mu_\phi^{n+\frac{1}{2}}, \tag{3.16b}$$

$$\frac{\rho^{n+1} - \rho^n}{\Delta t} + \lambda_2 \nabla \cdot (\tilde{\boldsymbol{u}}^{n+\frac{1}{2}} \check{\rho}) = M_2 \Delta \mu_\rho^{n+\frac{1}{2}}, \tag{3.16c}$$

$$\mu_\phi^{n+\frac{1}{2}} = -(\varepsilon + \theta) \Delta \phi^{n+\frac{1}{2}} + \sigma \phi^{n+\frac{1}{2}} + \check{V}_\phi^{n+\frac{1}{2}} r^{n+\frac{1}{2}}, \tag{3.16d}$$

$$\mu_\rho^{n+\frac{1}{2}} = -\eta \Delta \rho^{n+\frac{1}{2}} + \delta \rho^{n+\frac{1}{2}} + \check{V}_\rho^{n+\frac{1}{2}} r^{n+\frac{1}{2}}, \tag{3.16e}$$

$$r^{n+1} - r^n = \frac{1}{2}(\check{V}_\phi^{n+\frac{1}{2}}, \phi^{n+1} - \phi^n) + \frac{1}{2}(\check{V}_\rho^{n+\frac{1}{2}}, \rho^{n+1} - \rho^n), \tag{3.16f}$$

with the boundary condition

$$\tilde{\boldsymbol{u}}^{n+1}|_{\partial\Omega} = 0, \ \partial_{\boldsymbol{n}} \phi^{n+1}|_{\partial\Omega} = \partial_{\boldsymbol{n}} \rho^{n+1}|_{\partial\Omega} = 0, \ \partial_{\boldsymbol{n}} \mu_\phi^{n+1}|_{\partial\Omega} = \partial_{\boldsymbol{n}} \mu_\rho^{n+1}|_{\partial\Omega} = 0, \tag{3.17}$$

where

$$B(\boldsymbol{u}, \boldsymbol{v}) = (\boldsymbol{u} \cdot \nabla) \boldsymbol{v} + \frac{1}{2}(\nabla \cdot \boldsymbol{u}) \boldsymbol{v},$$

$$\check{\boldsymbol{u}} = \frac{3}{2}\boldsymbol{u}^n - \frac{1}{2}\boldsymbol{u}^{n-1}, \quad \check{\phi} = \frac{3}{2}\phi^n - \frac{1}{2}\phi^{n-1}, \quad \check{\rho} = \frac{3}{2}\rho^n - \frac{1}{2}\rho^{n-1},$$

$$\check{V}_\phi^{n+\frac{1}{2}} = \frac{\delta_\phi E_0(\check{\phi}, \check{\rho})}{\sqrt{E_0(\check{\phi}, \check{\rho})}}, \quad \check{V}_\rho^{n+\frac{1}{2}} = \frac{\delta_\rho E_0(\check{\phi}, \check{\rho})}{\sqrt{E_0(\check{\phi}, \check{\rho})}}.$$

Step 2: *Solve $\tilde{\boldsymbol{u}}^{n+1}, p^{n+1}$ by using*

$$\frac{\boldsymbol{u}^{n+1} - \tilde{\boldsymbol{u}}^{n+1}}{\Delta t} + \frac{1}{2}\nabla (p^{n+1} - p^n) = 0, \tag{3.18a}$$

$$\nabla \cdot \boldsymbol{u}^{n+1} = 0. \tag{3.18b}$$

with the boundary condition $\boldsymbol{u}^{n+1} \cdot \boldsymbol{n}|_{\partial\Omega} = 0$.

The unconditional energy stability of the Crank-Nicolson-type scheme can be easily proved in a similar way of handling the BDF2 scheme. Therefore, we leave the detailed proof for the interested readers.

4 Numerical experiments

We now present some numerical experiments to validate the theoretical results derived in the previous section and demonstrate the efficiency, unconditionally energy stability and accuracy of the proposed numerical scheme. In all the examples, we set the domain as $\Omega = [0; 2\pi]^2$. Here, we use the block-centered finite difference method to discretize the space. The main advantage of the block-centered finite difference method is not only that it approximates the phase functions with Neumann boundary conditions to second-order accuracy, but also it guarantees local mass conservation. If not specified, we use 128×128 grid in the following sections.

4.1 Accuracy and unconditional energy stability test

In this section, we focus on testing the convergence rate of the phase field functions ϕ and ρ, and the velocity $\boldsymbol{u}$. In addition, we provide a numerical test to illustrate the unconditional energy stability for the proposed scheme.

Table 1: The L^2 numerical error and convergence order at $t = 0.1$ based on the SAV approach and pressure correction method with the initial condition (4.1).

Δt	Error(ϕ)	Order	Error(ρ)	Order	Error(u)	Order	Error(v)	Order
5×10^{-3}	1.64E–05	–	8.46E–09	–	3.63E–11	–	3.63E–11	–
2.5×10^{-3}	4.87E–06	1.75	2.58E–09	1.72	9.01E–12	2.01	9.01E–12	2.01
1.25×10^{-3}	1.31E–06	1.89	6.91E–10	1.90	2.25E–12	2.00	2.25E–12	2.00
6.25×10^{-4}	3.38E–07	1.95	1.78E–10	1.96	5.65E–13	1.99	5.65E–13	1.99
3.125×10^{-4}	8.60E–07	1.98	4.52E–11	1.98	1.54E–13	1.87	1.54E–13	1.87

4.1.1 Accuracy test

To test the convergence rates of the proposed BDF2 scheme (3.1) and (3.7) in time, we choose the following initial conditions:

$$\begin{cases} \phi_0(x, y) = 0.5 + 0.4 \cos(x) \cos(y), \\ \rho_0(x, y) = 0.5 + 0.3 \cos(x) \cos(y), \\ \boldsymbol{u}_0(x, y) = 0. \end{cases} \quad (4.1)$$

where the parameters are chosen as follows:

$$M_1 = 0.01, \quad M_2 = 0.01, \quad \nu = 1, \quad \lambda_1 = 1e - 6, \quad \lambda_2 = 1e - 6, \quad \varepsilon = 0.05,$$

$$\beta = 0.05, \quad \alpha = 0.001, \quad \eta = 0.05, \quad \sigma = \frac{2}{\varepsilon}, \quad \delta = 10, \quad \theta = 0.0005, \quad C = 10000.$$

Since the exact solutions are not known, we measure the Cauchy error in time, which is similar to that of [45]. Specifically, the error between two different time step spacings Δt and $\frac{\Delta t}{2}$ is calculated by $\|e_\zeta\| = \|\zeta_{\Delta t} - \zeta_{\Delta t/2}\|$, where $\zeta = \phi$, ρ or $\boldsymbol{u}$. Additional data for ϕ^1, ρ^1 and $\boldsymbol{u}^1$ can be obtained by the first order scheme with an extremely fairly small time step. We present the L^2 errors of all the variables at time $t = 0.1$. We observe that the scheme is almost perfect second-order accuracy in time. The convergence order shown in Table 1 approaches 2 if the time step Δt tends to 0, which agrees with the theoretical analysis.

4.1.2 Unconditionally energy stable test

In this section, we will test the unconditional energy stability and the relation between the original and modified energy. Here, we take the initial condition as

$$\begin{cases} \phi_0(x, y) = 0.1 \cos(3x) + 0.4 \cos(y), \\ \rho_0(x, y) = 0.5 + 0.2 \cos(x) \cos(y), \\ \boldsymbol{u}_0(x, y) = 0. \end{cases} \quad (4.2)$$

The parameters are taken the same as those in 4.1.1.

On the one hand, Figure 1 and 2 show the original energy curves and modified energy curves with time steps $\Delta t = 0.05, 0.02, 0.01, 0.005, 0.002, 0.001$, respectively. The initial condition is taken as (4.2). We observe that these two figures show the decreasing trend of the original and modified energy with different time steps, and this phenomenon illustrates that both the original and modified energy numerically satisfy unconditional energy stability. On the other hand, we find that the energy stable curves are almost coincident with $\Delta t = 0.002$ and $\Delta t = 0.001$. This means that when we take the time step as less than 0.002, there is a small numerical error. We will take the time step as $\Delta t = 0.001$ in the following numerical experiments and take the original energy curve to describe the energy stability.

Besides, in Figure 3 the original and modified energy curves obtained by using the same time step $\Delta t = 0.001$ are shown in the same picture. We find that the two curves almost coincide, which indicates that the modified energy is a good approximation to the original one in discrete sense, though we do not have a serious proof theoretically.

4.2 Spinodal decomposition

In this example, we study a common phenomenon-phase separation behavior called spinodal decomposition. It can be studied by considering a homogeneous binary mixture, quenched into the unstable
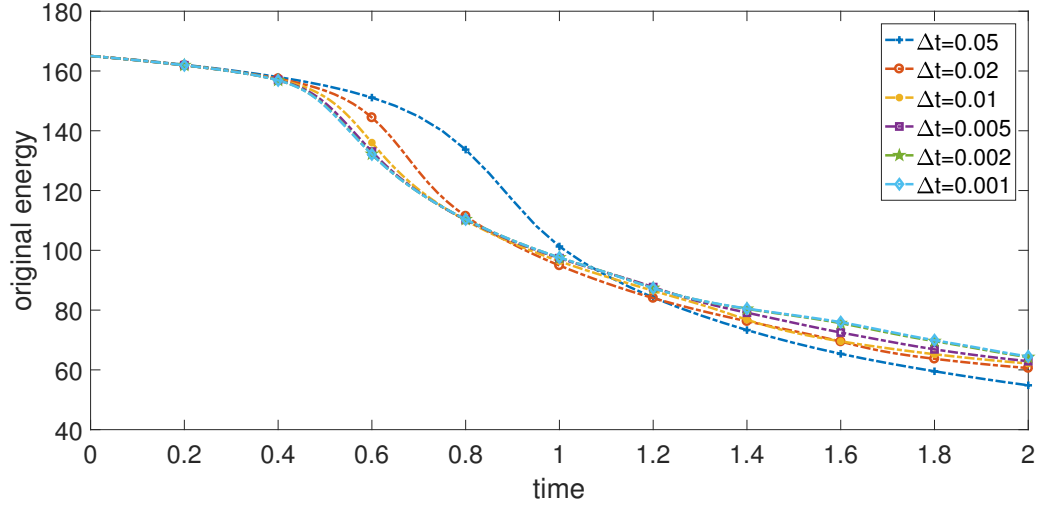
Figure 1: Time evolution of the original free energy functional for example (4.2). The energy curves with different time steps $\Delta t = 0.05,\ 0.02,\ 0.01,\ 0.005,\ 0.002,\ 0.001$ show monotone decay for this example.
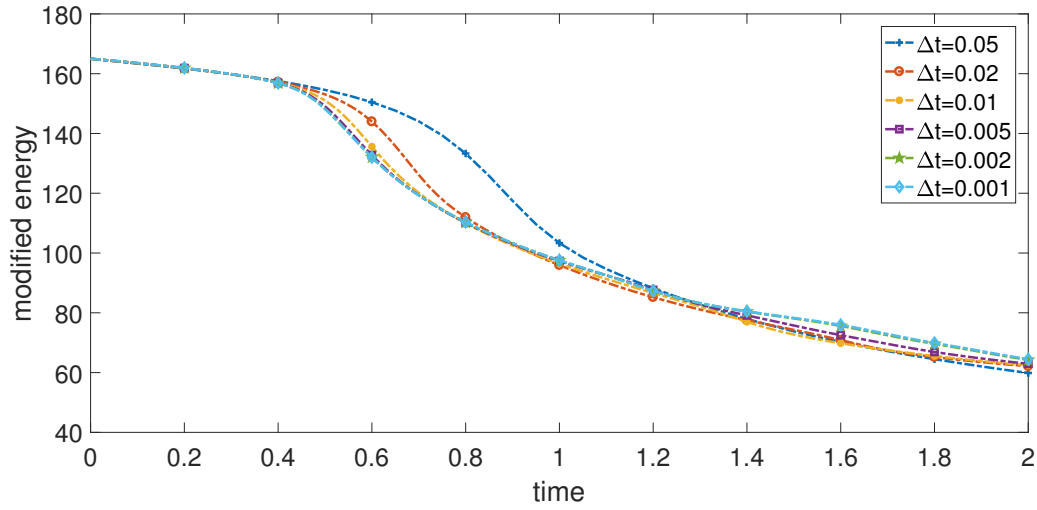

Figure 2: Time evolution of the modified free energy functional for example (4.2). The energy curves with different time steps $\Delta t = 0.05,\ 0.02,\ 0.01,\ 0.005,\ 0.002,\ 0.001$ show monotone decay for this example.
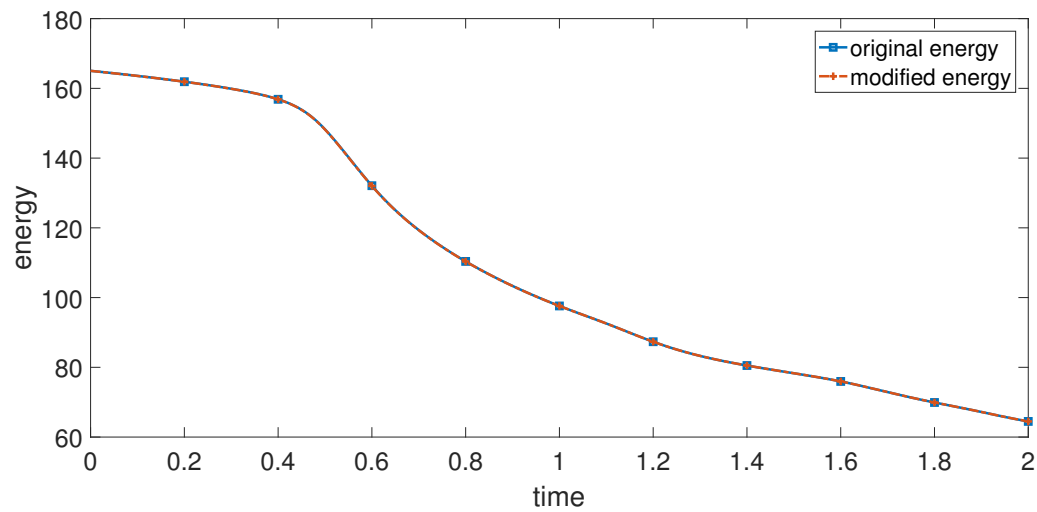
Figure 3: The comparison between the original and modified energy curves with time step $\Delta t = 0.001$. The energy curves show the same monotone decay for the original and modified energy.
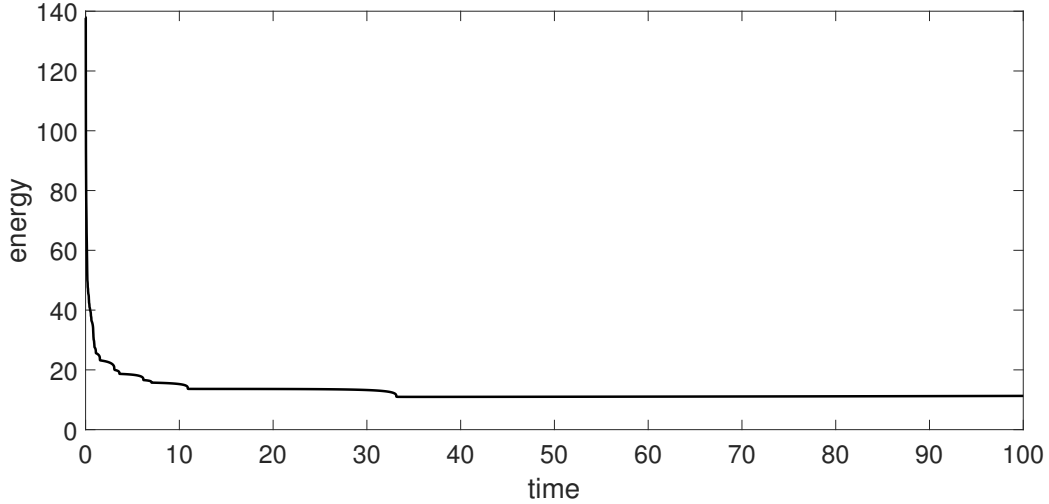
Figure 4: Time evolution of the free energy functional for the example (4.3).

part of its miscibility gap. After that, spinodal decomposition takes place, which reveals spontaneous growth of the concentration fluctuations that lead the system from the homogeneous to the two-phase state. Shortly after the phase separation starts, the domains of the binary components are formed and the interface between the two phases can be specified. Here, we take the random initial condition as

$$\begin{cases} \phi_0(x,y) = 0.4 + 0.001 \mathrm{rand}(x,y), \\ \rho_0(x,y) = 0.3, \\ \boldsymbol{u}_0(x,y) = 0, \end{cases} \tag{4.3}$$

where rand is a function that can generate a random number in $[0, 1]$. The parameters are taken as

$$M_1 = 1.0, \quad M_2 = 1.0, \quad \nu = 1, \quad \lambda_1 = 1e-6, \quad \lambda_2 = 1e-6, \quad \varepsilon = 0.05,$$
$$\beta = 0.05, \quad \alpha = 0.01, \quad \eta = 0.05, \quad \theta = 0.005, \quad \sigma = \frac{2}{\varepsilon}, \quad \delta = 10, \quad C = 10000.$$

In Figure 4, we present the evolution of the total free energy for this experiment. It is observed that the energy decays quickly in the initial stage (the random initial data becomes ordered), then the curve tends to flat and monotonically decreases slowly until it reaches steady state. This phenomenon agrees with those numerical results reported in literatures.

Figure 5 shows snapshots of ϕ, ρ a, and velocity $\boldsymbol{u}$, where we find the coarsening dynamics of the fluid component with less volume accumulates to small satellite drops everywhere. When the time evolves, the small drops will collide, merge and form drops with larger sizes. The final equilibrium solution is obtained around after $t = 35$, where all small bubbles accumulate into a large bubble.

4.3 Surfactant absorption

4.3.1 Surfactant uniformly distributed initially

In this example, we assume the fluid interface and the surfactant are initially uniformly distributed over the domain and the initial conditions are chosen as

$$\begin{cases} \phi_0(x,y) = 0.3 + 0.01 \cos(6x) \cos(6y), \\ \rho_0(x,y) = 0.1 + 0.01 \cos(6x) \cos(6y), \\ \boldsymbol{u}_0(x,y) = 0, \end{cases} \tag{4.4}$$

where the parameters are chosen as

$$M_1 = 1.0, \quad M_2 = 1.0, \quad \nu = 1, \quad \lambda_1 = 1e-6, \quad \lambda_2 = 1e-6, \quad \varepsilon = 0.05,$$
$$\alpha = 0.01, \quad \beta = 0.05, \quad \eta = 0.05, \quad \theta = 0.005, \quad \delta = 10, \quad \sigma = \frac{2}{\varepsilon}, \quad C = 10000.$$
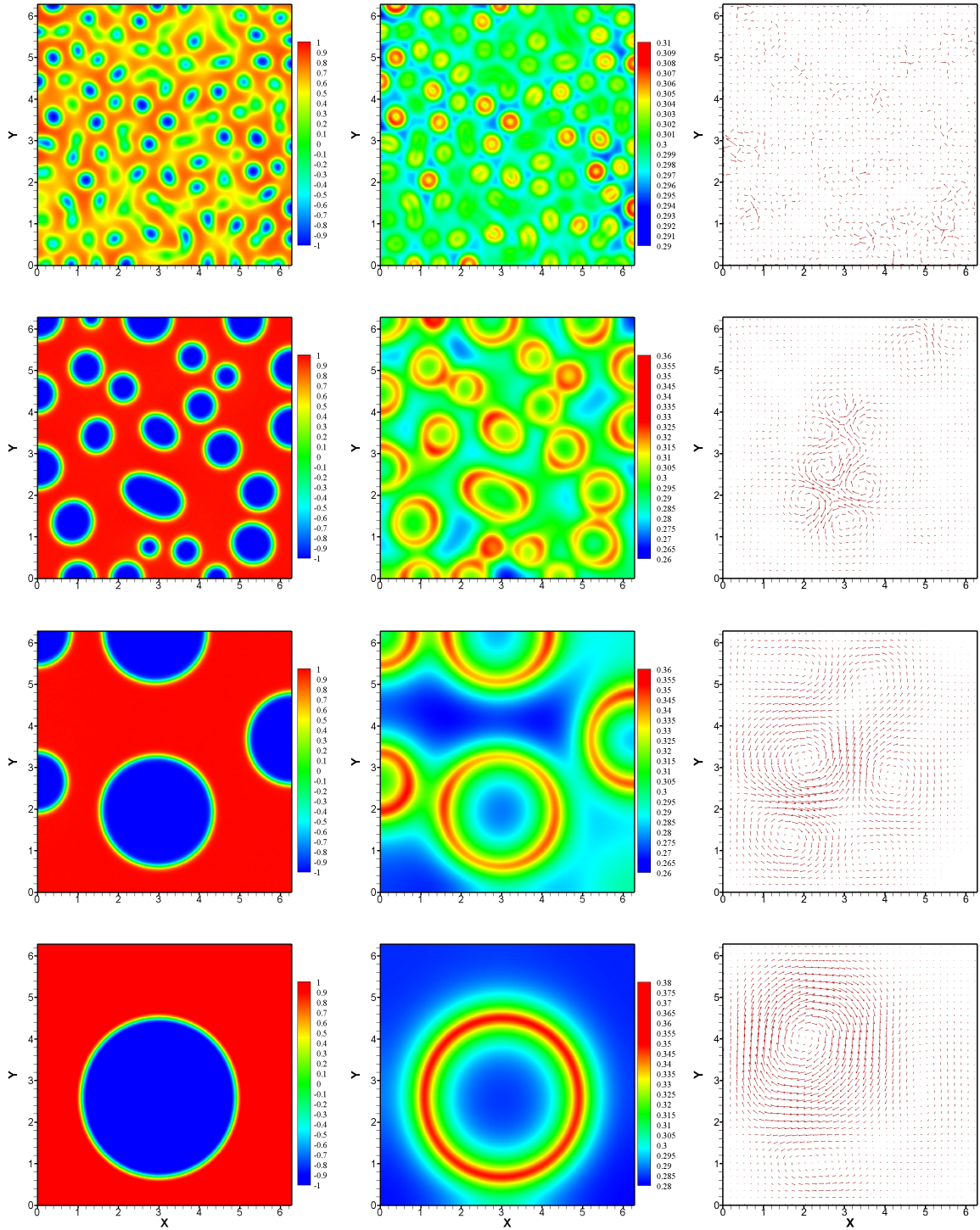
Figure 5: The phase transition process and velocity with the initial condition (4.3) at different times $t = 0.03, 0.2, 5, 50$, where the left column is the phase diagram for ϕ, the middle column is the phase diagram for ρ, and the right column is the velocity diagram for $\boldsymbol{u}$.

Figure 6 shows snapshots of the coarsening dynamics at $t = 0.1, 1, 3, 200$ for example (4.4). We can see that the surfactant is initially uniformly distributed in the domain with periodic structures. Then, quickly small structures merge to larger structures (some small structures are vanishing, while some ones are getting larger). Meanwhile, coarsening dynamics occur, driven by the coupling entropy energy term, and the surfactant is absorbed into the binary fluid interfaces so that a higher concentration appears near the interfaces than in other regions. The coupled velocity field is also presented in Figure 6.

Figure 7 displays the time evolution of the free energy functional for the examples (4.4). It is observed that the energy decreases with increasing time, which confirms the energy stability proved in the previous
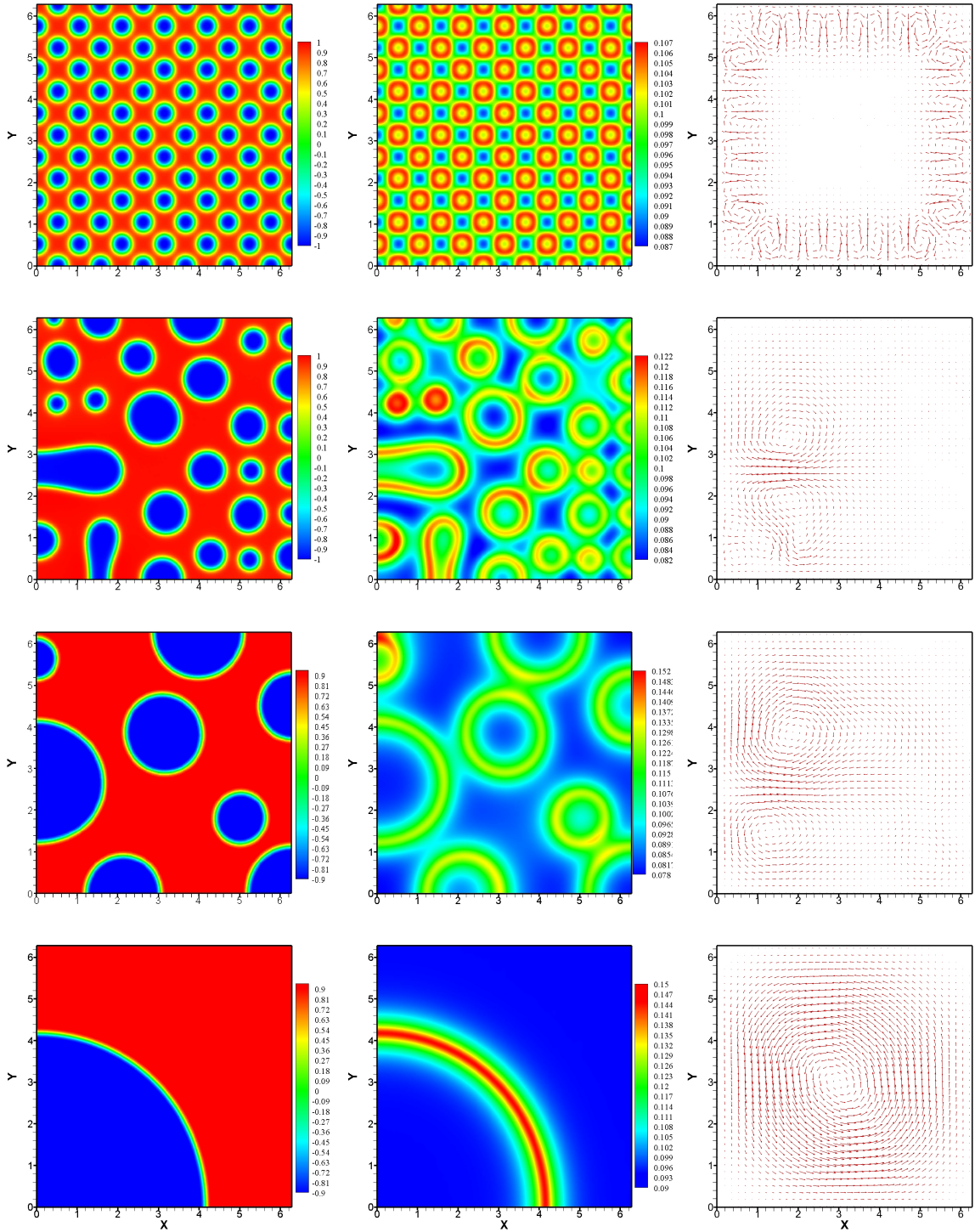
Figure 6: Snapshots of the phase variables ϕ and ρ and the velocity $\boldsymbol{u}$ are taken at $t = 0.1,\ 1,\ 3,\ 200$ for example (4.5), where the surfactants are initially distributed uniformly. The left panel is the profile of ϕ, the middle panel is the profile of ρ and the right panel is the profile of velocity $\boldsymbol{u}$.

section. In this experiment, the energy quickly goes down before $t = 10$, then it goes slowly down until the curve becomes almost flat after $t = 30$, which implies the system reaches equilibrium stage.
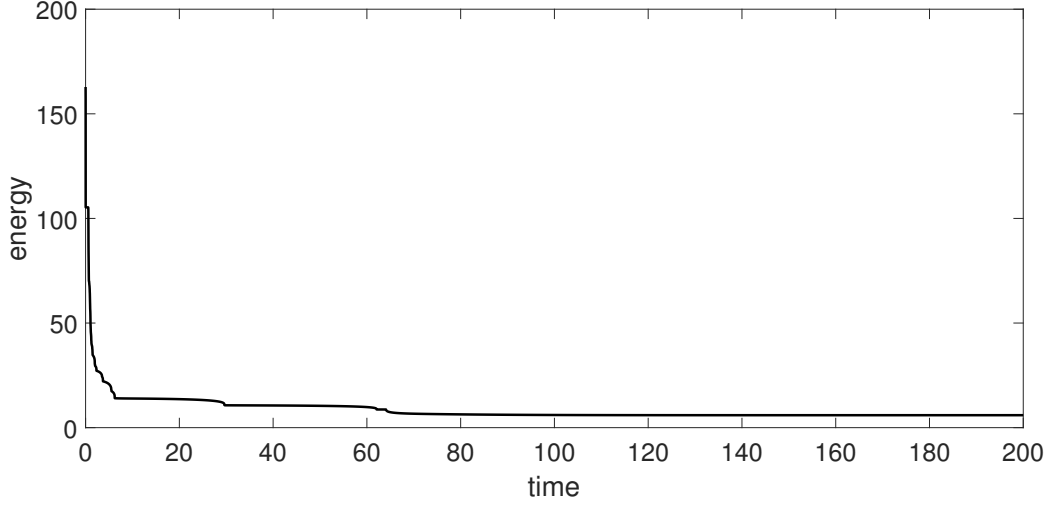
Figure 7: Time evolution of the free energy functional for example (4.4).
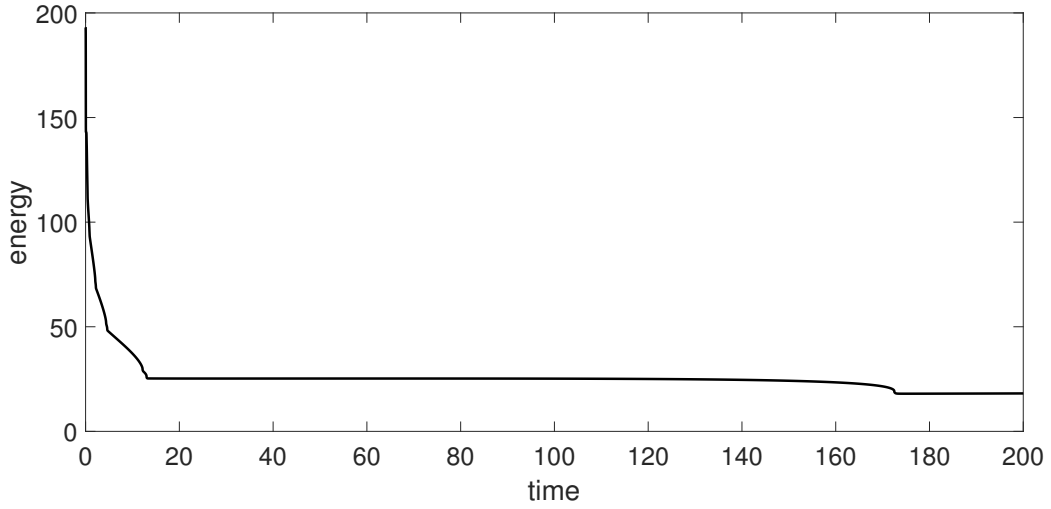
Figure 8: Time evolution of the free energy functional for example (4.5).

4.3.2 Surfactant locally distributed initially

Unlike example (4.4), in the last example, we assume the fluid interface and the surfactant field are initially mismatched over the domain. The initial conditions are chosen as

$$\begin{cases} \phi_0(x,y) = 0.1 + 0.01\cos(6x)\cos(6y), \\ \rho_0(x,y) = 0.8\exp\big(-\dfrac{(x-\pi)^2 + (y-\pi)^2}{1.25^2}\big), \\ \boldsymbol{u}_0(x,y) = 0, \end{cases} \qquad (4.5)$$

where the parameters are chosen as

$$M_1 = 0.1, \quad M_2 = 0.1, \quad \nu = 1, \quad \lambda_1 = 1e-6, \quad \lambda_2 = 1e-6, \quad \varepsilon = 0.05,$$

$$\alpha = 0.04, \quad \beta = 0.05, \quad \eta = 0.05, \quad \theta = 0.03, \quad \delta = 10, \quad \sigma = \frac{2}{\varepsilon}, \quad C = 10000.$$

Initially, the phase field variable ϕ is the same as that in the previous example, but the surfactant concentration variable ρ is locally distributed around the center of the domain. we plot the evolution of the energy curves in Figure 8, where the same phenomenon as the ones shown in the previous examples are observed. Figure 9 shows the snapshots of the dynamic behaviors of ϕ, ρ and $\boldsymbol{u}$ at various times. We observe that, since the surfactant is initially concentrated at the center, it takes longer for the surfactant to diffuse away from this center region. Consequently, during the early stage of the evolution, the higher
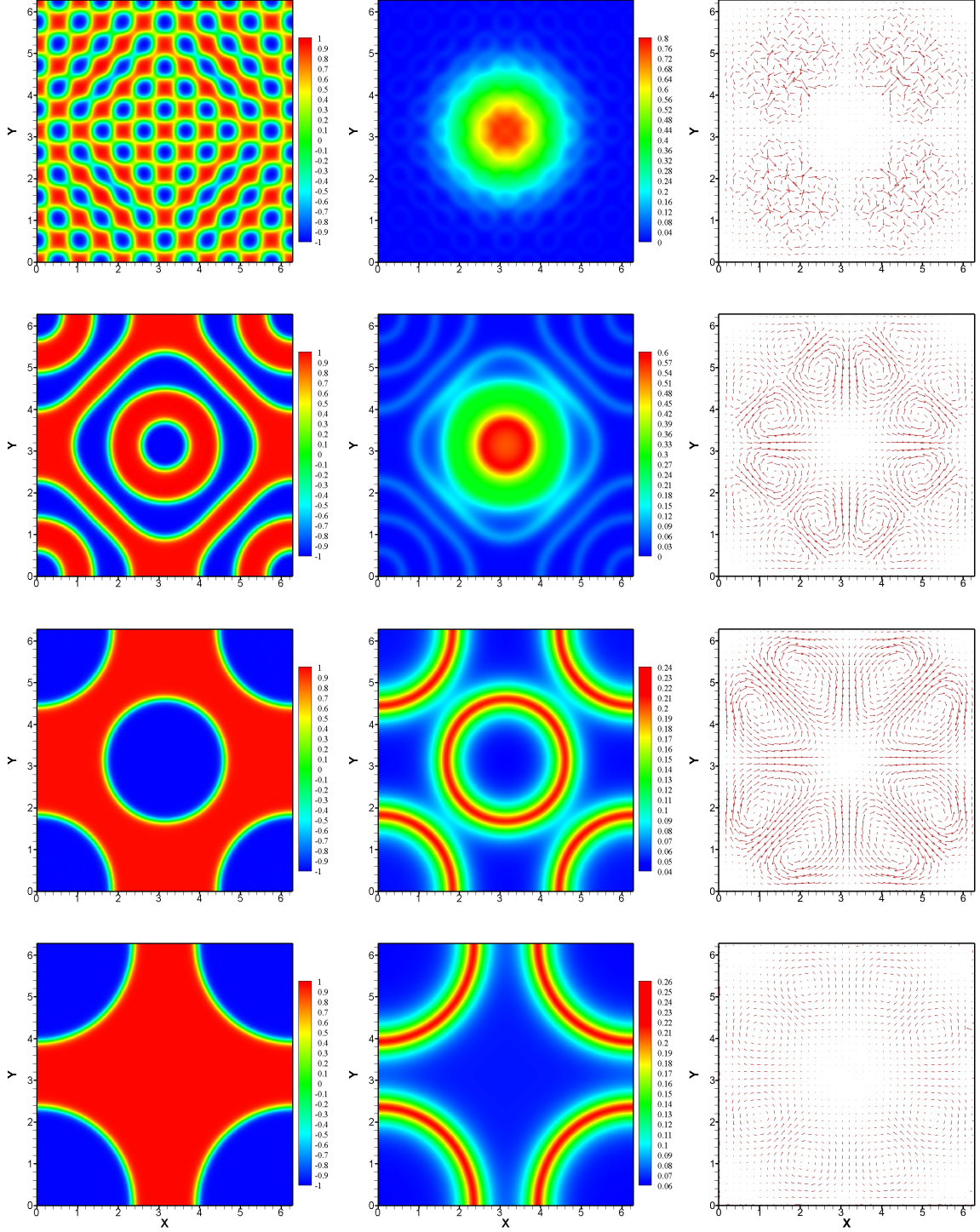
Figure 9: Snapshots of the phase variables ϕ and ρ are taken at $t = 0.2,\ 3,\ 100,\ 200$ for example (4.5), where the surfactants are initially distributed in a center circle. The left panel is the profile of ϕ, the middle panel is the profile of ρ and the right panel is the profile of velocity $\boldsymbol{u}$.

concentration of surfactant only appears around the center area of the domain. The surfactant completely diffuses and is absorbed into the binary fluid interfaces after $t = 200$.

5   Conclusion

In this paper, an efficient numerical scheme is developed for solving binary fluid-surfactant phase field model coupled with hydrodynamics. This scheme is designed by combining the pressure correction

method and the newly developed SAV approach. The obtained scheme is not only linear and second-order accurate in time but also decoupled about the two phase variables and velocity and pressure. We rigorously prove that the resulting linear system is unconditionally energy stable. Finally, various numerical examples are presented to validate the accuracy and stability of the proposed scheme.

6   Acknowledgement

References

[1] F. Boyer and S. Minjeaud. Numerical schemes for a three component Cahn-Hilliard model. *ESAIM Mathematical Modelling and Numerical Analysis*, 45(4):697–738, 2011.

[2] A. B. Branger and D. M. Eckmann. Accelerated arteriolar gas embolism reabsorption by an exogenous surfactant. *Anesthesiology*, 96(4):971–979, 2002.

[3] H. Chen, J. Mao, and J. Shen. Optimal error estimates for the scalar auxiliary variable finite-element schemes for gradient flows. *Numerische Mathematik*, 145:167–196, 2020.

[4] W. Chen, C. Wang, X. Wang, and S. M. Wise. Positivity-preserving, energy stable numerical schemes for the Cahn-Hilliard equation with logarithmic potential. *Journal of Computational Physics: X*, 3:1–29, 2019.

[5] Q. Cheng, C. Liu, and J. Shen. A new Lagrange multiplier approach for gradient flows. *Computer methods in applied mechanics and engineering*, 367(1):1–20, 2020.

[6] Q. Cheng, X. Yang, and J. Shen. Efficient and accurate numerical schemes for a hydro-dynamically coupled phase field diblock copolymer model. *Journal of Computational Physics*, 341(15):44–60, 2017.

[7] M. I. M. Copetti and C. M. Elliott. Numerical analysis of the Cahn-Hilliard equation with a logarithmic free energy. *Numerische Mathematik*, 63(1):39–65, 1992.

[8] A. E. Diegel and S. W. Walker. A finite element method for a phase field model of nematic liquid crystal droplets. *Communications in Computational Physics*, 25(1):155–188, 2017.

[9] L. Dong, C. Wang, H. Zhang, and Z. Zhang. A positivity-preserving, energy stable and convergent numerical scheme for the Cahn-Hilliard equation with a Flory-Huggins-deGennes energy. *Communications in Mathematical Physics*, 17(4):921–939, 2019.

[10] L. Dong, C. Wang, H. Zhang, and Z. Zhang. A positivity-preserving energy stable second order BDF scheme for the Cahn-Hilliard equation with variable interfacial parameters. *Communications in Computational Physics*, 28(3):967–998, 2020.

[11] D. J. Eyre. Unconditionally gradient stable time marching the Cahn-Hilliard equation. *Mrs Proceedings*, 529:39–46, 1998.

[12] X. Feng and A. Prohl. Numerical analysis of the Allen-Cahn equation and approximation for mean curvature flows. *Numerische Mathematik*, 94(1):33–65, 2003.

[13] G. J. Fix. Phase field models for free boundary problems. In A. Fasano and M. Primicerio, editors, *Free boundary problems: theory and applications*, volume 2, pages 580–589. Pitman, 1983.

[14] I. Fonseca, M. Morini, and V. Slastikov. Surfactants in foam stability: a phase-field model. *Archive for Rational Mechanics and Analysis*, 183(3):411–456, 2007.

[15] Lord Rayleigh F.R.S. On the theory of surface forces.II.Compressible fluids. *Philosophical Magazine Series 5*, 33(201):209–220, 1892.

[16] J. W. Gibbs. In *The scientific papes of J. Willard Gibbs*. Longmans, Green and Company, 1906.

[17] S. Gu, H. Zhang, and Z. Zhang. An energy-stable finite-difference scheme for the binary fluid-surfactant system. *Journal of Computational Physics*, 270(3):416–431, 2014.

[18] Y. Gu and J. Shen. Bound preserving and energy dissipative schemes for porous medium equation. *Journal of Computational Physics*, 410(1), 2020.

[19] F. Guilln-Gonzlez and G. Tierra. On linear schemes for a Cahn-Hilliard diffuse interface model. *Journal of Computational Physics*, 234(2):140–171, 2013.

[20] D. Han, A. Brylev, X. Yang, and Z. Tan. Numerical analysis of second order, fully discrete energy stable schemes for phase field models of two-phase incompressible flows. *Journal of Scientific Computing*, 70(3):965–989, 2017.

[21] A. J. James and J. Lowengrub. A surfactant-conserving volume-of-fluid method for interfacial flows with insoluble surfactant. *Journal of Computational Physics*, 201(2):685–722, 2004.

[22] G. Ji. A BDF2 energy-stable scheme for a general tensor based model of liquid crystals. *East Asian Journal of Applied Mathematics*, 2019.

[23] S. Khatri and A. K. Tornberg. An embedded boundary method for soluble surfactants with interface tracking for two-phase flows. *Journal of Computational Physics*, 256(1):768–790, 2014.

[24] S. Komura and H. Kodama. Two-order-parameter model for an oil-water-surfactant system. *Physical Review E*, 55(2):1722–1727, 1997.

[25] J. S. Langer. Models of pattern formation in first-order phase transitions. In G. Grinstein and G. Mazenko, editors, *Directions in Condensed Matter Physics. Directions in Condensed Matter Physics. Series: Series on Directions in Condensed Matter Physics. Series on Directions in Condensed Matter Physics*, volume 1, pages 165–186. World Scientific, 1986.

[26] M. Laradji, H. Guo, M. Grant, and M. J. Zuckermann. The effect of surfactants on the dynamics of phase separation. *Journal of Physics Condensed Matter*, 4(4):6715–6728, 1992.

[27] X. Li and J. Shen. Stability and error estimates of the SAV Fourier-spectral method for the phase field crystal equation. *Advances in Computational Mathematics*, 2020.

[28] X. Li, J. Shen, and H. Rui. Energy stability and convergence of SAV Block-Centered finite difference method for gradient flows. *Mathematics of Computation*, 88(319):2047–2068, 2019.

[29] H. Liu and Y. Zhang. Phase-field modeling droplet dynamics with soluble surfactants. *Journal of Computational Physics*, 229(24):9166–9187, 2010.

[30] D. Myers. Fluid surfaces an interfaces. In *Surfactant science and technology*, pages 80–106. Wiley-Interscience, 2005.

[31] J. Shen, C. Wang, X. Wang, and S. M. Wise. Second-order convex splitting schemes for gradient flows with Ehrlich-Schwoebel type energy: application to thin film epitaxy. *SIAM Journal on Numerical Analysis*, 50(1):105–125, 2012.

[32] J. Shen and J. Xu. Convergence and error analysis for the scalar auxiliary variable (SAV) schemes to gradient flows. *SIAM Journal on Numerical Analysis*, 56(5):2895–2912, 2018.

[33] J. Shen and J. Xu. Unconditionally bound preserving and energy dissipative schemes for a class of Keller-lsegel equations. *SIAM Journal on Numerical Analysis*, 58(3):1674–1695, 2020.

[34] J. Shen, J. Xu, and J. Yang. A new class of efficient and robust energy stable schemes for gradient flows. *SIAM Review*, 61(3):474–506.

[35] J. Shen, J. Xu, and J. Yang. The scalar auxiliary variable (SAV) approach for gradient flows. *Journal of Computational Physics*, 353(15):407–416, 2018.

[36] J. Shen and X. Yang. Numerical approximations of Allen-Cahn and Cahn-Hilliard equations. *Discrete and Continuous Dynamical Systems*, 28(4):1669–1691, 2010.

[37] J. Stefan. Über die theorie der eisbildung. *Monatshefte Für Mathematik Und Physik*, 1(1):1–6, 1890.

[38] K. E. Teigen, P. Song, J. Lowengrub, and A. Voigt. A diffuse-interface method for two-phase flows with soluble surfactants. *Journal of Computational Physics*, 230(2):375–393, 2011.

[39] C. Teng, I. Chern, and M. Lai. Simulating binary fluid-surfactant dynamics by a phase field model. *Discrete and Continuous Dynamical Systems - Series B*, 17(4):1289–1307, 2012.

[40] T. Teramoto and F. Yonezawa. Droplet growth dynamics in a water/oil/surfactant system. *Journal of Colloid and Interface Science*, 235(2):329–333, 2001.

[41] O. Theissen and G. Gompper. Lattice-Boltzmann study of spontaneous emulsification. *The European Physical Journal B - Condensed Matter and Complex Systems*, 11(1):91–100, 1999.

[42] R. G. M. van der Sman and S. van der Graaf. Diffuse interface model of surfactant adsorption onto flat and droplet interfaces. *Rheologica Acta*, 46(1):3–11, 2006.

[43] J. D. van der Waals. The thermodynamic theory of capillarity under the hypothesis of a continuous variation of density. *Journal of Statistical Physics*, 20(2):200–244, 1979.

[44] C. Wang and S. M. Wise. An energy stable and convergent finite-difference scheme for the modified phase field crystal equation. *SIAM Journal of Numerical Analysis*, 49(3):945–969, 2011.

[45] S. Wise, J. Kim, and J. Lowengrub. Solving the regularized, strongly anisotropic Cahn-Hilliard equation by an adaptive nonlinear multigrid method. *Journal of Scientific Computing*, 226(1):414446, 2007.

[46] X. Wu, G. J. van Zwieten, and K. G. van der Zee. Stabilized second-order convex splitting schemes for Cahn-Hilliard models with application to diffuse-interface tumor-growth models. *International Journal for Numerical Methods in Biomedical Engineering*, 30(2):180–203, 2017.

[47] C. Xu, C. Chen, X. Yang, and X. He. Numerical approximations for the hydrodynamics coupled binary surfactant phase field model: second-order, linear, unconditionally energy stable schemes. *Communications in Mathematical Sciences*, 17(3):835–858, 2020.

[48] Y. Yan, W. Chen, C. Wang, and S. M. Wise. A second-order energy stable BDF numerical scheme for the Cahn-Hilliard equation. *Communications in Computational Physics*, 23(2):572–602, 2018.

[49] X. Yang. Linear, first and second-order, unconditionally energy stable numerical schemes for the phase field model of homopolymer blends. *Journal of Computational Physics*, 327(15):294–316, 2016.

[50] X. Yang. Numerical approximations for the Cahn-Hilliard phase field model of the binary fluid-surfactant system. *Journal of Scientific Computing*, 74(3):1533–1553, 2018.

[51] X. Yang and L. Ju. Efficient linear schemes with unconditional energy stability for the phase field elastic bending energy model. *Computer Methods in Applied Mechanics and Engineering*, 315(1):691–712, 2017.

[52] X. Yang and L. Ju. Linear and unconditionally energy stable schemes for the binary fluid-surfactant phase field model. *Computer Methods in Applied Mechanics and Engineering*, 318(1):1005–1029, 2017.

[53] X. Yang, J. Zhao, and Q. Wang. Numerical approximations for the molecular beam epitaxial growth model based on the invariant energy quadratization method. *Journal of Computational Physics*, 333(15):104–127, 2017.

[54] X. Yang, J. Zhao, Q. Wang, and J. Shen. Numerical approximations for a three-component Cahn-Hilliard phase-field model based on the invariant energy quadratization method. *Mathematical Models and Methods in Applied Sciences*, 27(11):1993–2030, 2017.

[55] C. Zhang, H. Li, X. Zhang, and L. Ju. Linear and unconditionally energy stable schemes for the multi-component two-phase diffuse interface model with Peng-Robinson equation of state. *Communications in Computational Physics*, 26(4):1071–1097, 2019.

[56] J. Zhao, Q. Wang, and X. Yang. Numerical approximations for a phase field dendritic crystal growth model based on the invariant energy quadratization approach. *International Journal for Numerical Methods in Engineering*, 110(3):279–300, 2017.

[57] G. Zhu, J. Kou, S. Sun, J. Yao, and A. Li. Decoupled, energy stable schemes for a phase-field surfactant model. *Computer Physics Communications*, 233:67–77, 2018.

[58] G. Zhu, J. Kou, S. Sun, J. Yao, and A. Li. Numerical approximations of a phase-field surfactant model with fluid flow. *Journal of Scientific Computing*, 80:223–247, 2019.